



Published in final edited form as:

Cell Rep. 2021 January 26; 34(4): 108656. doi:10.1016/j.celrep.2020.108656.

FOS licenses early events in stem cell activation driving skeletal muscle regeneration

Albert E. Almada^{1,2,3,5,*}, **Naftali Horwitz**^{1,2,3}, **Feodor D. Price**¹, **Alfredo E. Gonzalez**^{1,2}, **Michelle Ko**^{1,2}, **Ozge Vargel Bolukbasi**¹, **Kathleen A. Messemer**^{1,2}, **Sonia Chen**¹, **Manisha Sinha**^{1,3,4}, **Lee L. Rubin**¹, **Amy J. Wagers**^{1,2,3,6,*}

¹Department of Stem Cell and Regenerative Biology, Harvard University and Harvard Stem Cell Institute, Cambridge, MA 02138, USA

²Paul F. Glenn Center for the Biology of Aging, Harvard Medical School, Boston, MA 02115, USA

³Joslin Diabetes Center, Boston, MA 02215, USA

⁴Present address: Elevian, Inc., Pagliuca Harvard Life Lab, 127 Western Ave., Allston, MA 02134, USA

⁵Present address: Departments of Orthopedic Surgery and Stem Cell Biology and Regenerative Medicine at the University of Southern California (USC), Keck School of Medicine of USC, Los Angeles, CA 90033, USA

⁶Lead contact

SUMMARY

Muscle satellite cells (SCs) are a quiescent (non-proliferative) stem cell population in uninjured skeletal muscle. Although SCs have been investigated for nearly 60 years, the molecular drivers that transform quiescent SCs into the rapidly dividing (activated) stem/progenitor cells that mediate muscle repair after injury remain largely unknown. Here we identify a prominent FBJ osteosarcoma oncogene (*Fos*) mRNA and protein signature in recently activated SCs that is rapidly, heterogeneously, and transiently induced by muscle damage. We further reveal a requirement for FOS to efficiently initiate key stem cell functions, including cell cycle entry, proliferative expansion, and muscle regeneration, via induction of “pro-regenerative” target genes that stimulate cell migration, division, and differentiation. Disruption of one of these *Fos/AP-1* targets, NAD(+)-consuming mono-ADP-ribosyl-transferase 1 (*Art1*), in SCs delays cell cycle entry and impedes progenitor cell expansion and muscle regeneration. This work uncovers an

This is an open access article under the CC BY-NC-ND license (<http://creativecommons.org/licenses/by-nc-nd/4.0/>).

*Correspondence: aalmada@usc.edu (A.E.A.), amy_wagers@harvard.edu (A.J.W.).

AUTHOR CONTRIBUTIONS

A.E.A. conceived the project, designed the study, performed experiments, analyzed and interpreted data, wrote the manuscript, and secured funding. N.H., A.E.G., M.K., K.A.M., and S.C. assisted with muscle SC isolation, tissue sectioning, IF staining and analysis, and genotyping. F.D.P. and L.L.R. designed and performed IF staining and p38i treatment of single fibers. O.V.B. performed ChIP-qPCR experiments and analyzed the resulting data. M.S. generated microarray data representing fresh and cultured SCs. A.E.A. and N.H. performed microarray and RNA-seq bioinformatics analyses. A.J.W. supervised the study, designed experiments, interpreted data, wrote the manuscript, and secured funding. All authors approved and provided feedback on the manuscript.

SUPPLEMENTAL INFORMATION

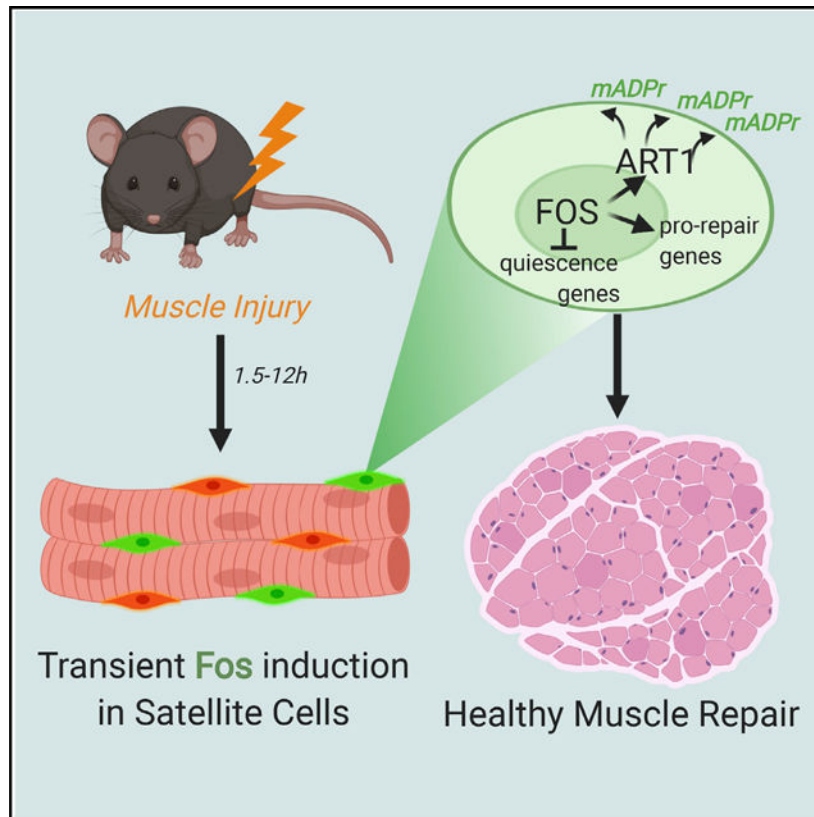
Supplemental Information can be found online at <https://doi.org/10.1016/j.celrep.2020.108656>.

early-activated FOS/ART1/mono-ADP-ribosylation (MARylation) pathway that is essential for stem cell-regenerative responses.

In Brief

How adult stem cells are activated to repair tissues and organs after injury remains one of the greatest mysteries in regenerative biology. Almada et al. reveal a FOS-driven “pro-regenerative” transcriptional gene network, including the NAD(+)-dependent mono-ADP-ribosylating (MARylating) enzyme *Art1*, that drives effective muscle stem cell activation and muscle repair.

Graphical Abstract



INTRODUCTION

Skeletal muscle regeneration has intrigued investigators for centuries, but it was only roughly 60 years ago that “satellite cells” were first proposed as tissue-resident stem/progenitor cells responsible for repairing postnatal skeletal muscle (Mauro, 1961). Recent work has confirmed an absolute requirement for satellite cells (SCs) to elicit a robust reparative muscle injury response (Lepper et al., 2011; Sambasivan et al., 2011).

SCs in uninjured muscle typically exist in a quiescent (non-dividing) state beneath the basal lamina of muscle fibers and are marked by expression of the paired box 7 (PAX7)

transcription factor (Mauro, 1961; Seale et al., 2000). Upon muscle damage, PAX7+ SCs are activated, induce myogenic determination factor 1 (MYOD1) (Zammit et al., 2004), and migrate toward sites of damage, where they transition to a highly proliferative state capable of fusion to repair injured fibers. SCs also self-renew during the muscle injury response, ensuring maintenance of the stem cell pool to meet future regenerative demands (Cerletti et al., 2008; Collins et al., 2005; Kuang et al., 2007).

SCs are recruited for muscle repair in response to various stressors, including stretching, denervation, exercise-induced micro-trauma, and more severe myofiber destruction. However, the molecular driver(s) that control the awakening (activation) of dormant SCs and their transition into proliferating precursor cells that actively participate in muscle repair remain largely unknown. Recent data indicate that cell cycle entry from quiescence (i.e., time to first cell division) is a rate-limiting step in SC activation and that the speed at which SCs overcome this barrier correlates directly with the kinetics and efficiency of muscle regeneration (Rocheteau et al., 2012; Rodgers et al., 2014). Moreover, defects in the SC transition from quiescence to activation contribute to the decline of muscle repair in aged and pathologically diseased skeletal muscle (Chakkalakal et al., 2012; Dumont et al., 2015). These observations highlight the importance of elucidating the molecular triggers of SC activation in order to advance future therapies that can improve regenerative function and preserve physical robustness in vulnerable populations.

SCs can be isolated directly from skeletal muscle using combinatorial cell surface marker expression and fluorescence-activated cell sorting (FACS) (Cerletti et al., 2008; Montarras et al., 2005; Sacco et al., 2008; Sherwood et al., 2004). Upon intramuscular transplantation, such freshly isolated SCs (fresh SCs) rapidly and efficiently engage in muscle repair and also colonize the SC niche. However, the proliferating progeny of these cells, commonly referred to as activated SCs or myoblasts, are substantially less efficient in these same regenerative assays. These data suggest that SCs isolated from uninjured skeletal muscle are primed with a specialized gene expression program that enables their enhanced migration, proliferation, and differentiation in response to tissue injury. Recent reports have cataloged many differences in the transcriptional profile of fresh SCs compared with their *in vivo* quiescent counterparts and indicate that the isolation procedure is likely perceived by SCs as a damage signal, leading to rapid suppression of quiescence-associated genes and induction of other genes that may include critical drivers of muscle stem cell activity (Machado et al., 2017; van den Brink et al., 2017; van Velthoven et al., 2017). Among these induced genes, the activator protein 1 (AP-1) family of mRNAs is particularly noted for its enrichment in fresh SCs. However, the extent to which AP-1 transcription factors function in stem cells to instruct adult regenerative responses, and the downstream network of target genes driving their potentially critical “regenerative” activities, remains unexplored.

In this study, we uncovered FOS/AP-1 as one of the earliest known transcriptional effectors of adult muscle SC activation whose immediate and transient activity is required to efficiently initiate the SC regenerative program, including rapid entry into the cell cycle, expansion of cell numbers, and regeneration of muscle fibers after injury. We further identify a suite of transcriptional targets induced by FOS/AP-1 and mechanistically highlight one of these, the mono-ADP-ribosyl-transferase 1 (*Art1*) enzyme, revealing a previously

hidden post-translational mechanism (mono-ADP-ribosylation [MARylation]) that re-wires quiescent SCs for regenerative fates. This work demonstrates the seminal contribution of transient, “early” stem cell activation signals to ensuring long-term muscle regenerative output.

RESULTS

Abundant *Fos* mRNA is a feature of SCs freshly isolated from uninjured skeletal muscle

We began by comparing the transcriptomes of non-dividing, fresh SCs recently isolated from uninjured mouse muscle tissue with those of proliferating SCs cultured for 5 days in myogenic growth medium (GM), with the latter typically displaying poorer engraftment efficiency when transplanted into recipient muscle (Montarras et al., 2005). Fresh and cultured SCs were isolated by FACS using negative selection for surface antigens expressed by non-myogenic cells ($Sca1^{-}/CD31^{-}/CD45^{-}/CD11b^{-}/Ter119^{-}$) and positive selection for the SC markers β 1-integrin and CXCR4 (Figure 1A; Maesner et al., 2016; Sherwood et al., 2004). In total, we identified 736 differentially expressed genes (DEGs) that were changed more than 2-fold with a false discovery rate (FDR) of less than 0.02. 669 genes were enriched in fresh SCs, and 67 genes were enriched in their cultured counterparts. Filtering the 669 DEGs enriched in fresh SCs for annotated transcription factors (TFs), we identified 45 unique TFs (Figure 1B; Table S1).

Several of the 45 TFs we identified as enriched in fresh SCs are known regulators of SC quiescence, including *Pax7*, *Cebp β* , *HeyL*, and *Id3* (Figure 1C), consistent with the notion that fresh SCs from uninjured muscle are closer to a quiescent state compared with cultured SCs. Other notable regulators included the cyclic AMP (cAMP) signaling proteins *Crem* and *Creb5* and various mitogen-activated protein kinase (MAPK) targets such as *Myc*, *RelA*, *Nr4a1*, and *Ddit3* (Table S1). Finally, the TFs that were the most enriched, as defined by fold change, in fresh SCs were from the AP-1 complex (*Fos*, *Fosb*, *Jun*, *JunB*, and *JunD*) and various AP-1-associated factors (*Mafk*, *Mafk*, *Atf3/4*, and *Egr1/2*). In particular, *Fos* was the most enriched (~65-fold; Figure 1C) TF transcript in fresh SCs, an observation confirmed by the higher levels of FOS protein detected in fresh SCs from uninjured as opposed to injured muscle (Figure S1). In addition, *Fos* transcripts were among the most abundant mRNAs in fresh SCs (Figure 1D), and the *Fos* gene locus was associated with a histone H3 lysine 27 acetylation (H3K27ac)-marked active enhancer domain (Figure 1F). Analysis of previously published datasets showed that *Fos* mRNA also ranked among the top enriched TF transcripts in fresh SCs (relative to their *in vivo* or *ex vivo* proliferating counterparts) when these cells were isolated by Vcam1 (Liu et al., 2013) or α 7-integrin expression (Ryall et al., 2015) and in human fresh SCs identified by β 1-integrin and epidermal growth factor receptor (EGFR) expression (Charville et al., 2015; Figure S2). In contrast, *Fos* mRNA expression was suppressed in actively proliferating SCs (5-day-cultured), committed myoblasts, and terminal myotubes *in vitro* (Figure 1E). Thus, high *Fos* mRNA levels are a conserved feature of fresh SCs in mice and humans, independent of the SC markers used for cell isolation, raising the possibility that FOS activity may be required to direct early stem cell activation events needed for efficient regenerative myogenesis.

FOS is transiently and heterogeneously induced in SCs within hours after muscle trauma

To gain insight into the dynamics of FOS protein expression in response to muscle damage, we analyzed previously described FOS^{GFP} transgenic mice (Figure 2A) that express a single transgenic copy of a Fos^{GFP} fusion protein controlled by a minimal *Fos* promoter (Barth et al., 2004). Flow cytometry analysis of fresh SCs from uninjured muscle of these mice showed ~50% (based on a fluorescence minus one [FMO] control) of the SC pool marked by GFP expression (Figures 2B and 2C). To ascertain whether FOS protein is expressed in quiescent SCs or, instead, whether it might be induced during the early stages of activation (e.g., during the process of SC isolation for FACS; Machado et al., 2017; van den Brink et al., 2017; van Velthoven et al., 2017), we next evaluated PAX7 and FOS protein expression in fresh myofiber-associated SCs prepared from muscle using standard methods or after a “pre-fix” step designed to maintain the “pre-dissociation” state of these cells (Figure 2A). Interestingly, FOS was undetectable in most SCs associated with single fibers from pre-fixed muscle, whereas ~60% of the PAX7+ SCs from fibers prepared using standard post-dissociation fixation strategies showed detectable FOS (Figures 2D and 2E).

To define the kinetics of FOS induction by SCs *in vivo*, we next performed cardiotoxin (CTX; 10 μ M) injuries in *tibialis anterior* (TA) muscles of adult mice. We isolated muscles before (T0) or 1.5, 3, 12, 24, or 120 h after injury and immunostained for FOS (Figures S3A and S3B). FOS was generally undetectable in uninjured muscle but was transiently induced within 1.5–3 h after CTX injection (Figure S3B). FOS levels subsequently declined, returning to baseline by 120 h after injury (Figure S3B). Similar results were obtained when immunostaining for GFP protein in TA muscles from Fos^{GFP} mice before and after CTX injury (Figures S4A and S4B). Co-staining for FOS and PAX7 0, 1.5, and 12 h after injury confirmed minimal detection of FOS protein in SCs in the absence of muscle damage and rapid induction of FOS in ~60% of SCs within 1.5 h after injury (Figures 2F–2H). By 12 h after injury, however, FOS was detected in only about 15% of PAX7+ cells. We also noted FOS protein expressed in PAX7-negative (non-satellite) cells after CTX injection, suggesting that myonuclei and/or other mononuclear cells in muscle also induce FOS with similar kinetics in response to injury. These data demonstrate that FOS is induced heterogeneously in SCs very early in the response to muscle damage, consistent with the possibility that FOS may function to instruct SC fate decisions that trigger rapid muscle-regenerative responses.

Fos^{GFP} marks a subset of SCs with enhanced regenerative activity

To evaluate the functional consequences of induced FOS expression in early-activated SCs, we took advantage of our capacity to use GFP as a surrogate in FOS^{GFP} transgenic mice to isolate, from enzymatically dissociated muscle, subsets of SCs that differ in FOS levels (Figure 3A). We confirmed that fresh SCs from Fos^{GFP} and wild-type littermates showed similar kinetics of *Fos* induction, similar global transcriptional profiles (including expression of FOS/AP-1 targets), and a similar capacity to enter the cell cycle from quiescence and expand in culture, indicating that the presence of the Fos^{GFP} fusion protein preserves normal SC behavior and FOS/AP-1 transcriptional activity in these cells (Figure S4).

Following this phenotypic and functional validation of the Fos^{GFP} reporter system, we utilized Fos^{GFP} mice to separate fresh FOS^{GFP+} and FOS^{GFP-} SCs and determine whether they differed in their capacity to induce MYOD upon myogenic cell culture. After 6 h, 73% ± 2% of nuclei in cultures seeded with FOS^{GFP+} cells were MYOD+ compared with only 54% ± 4% in cultures seeded with FOS^{GFP-} cells (Figure 3B). These data suggest that FOS-expressing SCs exhibit a greater propensity for entering the early stages of activation. We next tested the colony formation capacity of single FOS^{GFP+} and FOS^{GFP-} SCs, a readout that provides dual insights into cell survival after FACS and clonal expansion potential. We detected no significant differences in the frequency with which FOS^{GFP+} and FOS^{GFP-} SCs formed viable myogenic colonies (Figure 3C, left); however, wells seeded initially with a single FOS^{GFP+} cell more frequently generated large colonies (>200 cells per well) after 7 days in culture (Figure 3C, right). To test whether the larger colonies formed by FOS^{GFP+} SCs reflected enhanced proliferation kinetics, we isolated FOS^{GFP+} and FOS^{GFP-} SCs and cultured them for 3 or 6 days (Figure 3D). Interestingly, after 3 days in culture, 5-Ethynyl-2'-deoxyuridine (EdU) incorporation following a 3-h EdU pulse was 3-fold greater in cultures initiated with FOS^{GFP+} SCs compared with FOS^{GFP-} SCs; however, this difference in cycling kinetics was not seen when cultures were pulsed with EdU after 6 days in culture (Figure 3D). These data suggest that FOS-expressing SCs exhibit an accelerated rate of initial entry into the cell cycle from quiescence, a rate-limiting step in regenerative myogenesis that typically requires several days (Rodgers et al., 2014).

Finally we tested whether the enhanced stem cell activation properties of fresh FOS^{GFP+} SCs might translate into a more rapid regenerative response *in vivo*. We transplanted 3,000 FOS^{GFP+} or FOS^{GFP-} fresh SCs into TA muscles of pre-injured *mdx* mice (CTX, 10 μM) and quantified the total number of DYSTROPHIN+ fibers formed after 3 weeks. Indeed, FOS^{GFP+} SCs displayed a more robust regenerative response in this *in vivo* assay, producing ~90% (range, 59%–124%) more engrafted DYSTROPHIN+ fibers than equal numbers of similarly transplanted FOS^{GFP-} SCs (Figures 3E–3G). These data argue that SCs expressing FOS^{GFP} are primed to initiate a rapid burst of proliferation that enhances clonal expansion and increases the contribution of these cells to the repair of damaged muscle.

Fos^{GFP+} SCs exhibit a pro-regenerative transcriptional gene signature

To decode the molecular mechanisms driving the enhanced regenerative activity of FOS-expressing SCs, we performed RNA sequencing (RNA-seq) analysis in early-activated Fos^{GFP+} and Fos^{GFP-} SCs freshly isolated from Fos^{GFP} mice (Figure 4A). As anticipated, principal-component analysis (PCA) distinguished Fos^{GFP+} from Fos^{GFP-} SCs, consistent with the notion that FOS marks a molecularly unique subset within the SC pool (Figure S5A). We identified 2,882 and 505 genes enriched (>1.5-fold changed with FDR < 0.05) in Fos^{GFP+} or Fos^{GFP-} SCs, respectively (Figure 4B; Table S2). We observed no differences in *Pax7*, *Spry1*, or *Myf5* mRNA levels between the two populations (Figure 4C), indicating that Fos^{GFP+} Fresh SCs represent a SC state that only partially overlaps with those described previously (Chakkalakal et al., 2014; Kuang et al., 2007; Rocheteau et al., 2012). Interestingly, some of the genes enriched in Fresh Fos^{GFP+} SCs have been reported to have roles in SC proliferation/self-renewal and differentiation (Figure 4C; Figure S5B), whereas

several known quiescence-related genes were enriched in the Fos^{GFP-} sub-fraction of fresh SCs (Figure 4C; Figure S5D).

An unbiased search for Gene Ontology (GO) terms and pathways associated with Fos^{GFP+} SCs revealed gene sets involved in regulation of metabolic and cellular processes (Figure S5C; Table S2) and pathways critical for stem cell migration, proliferation, and differentiation (i.e., *RAC/PI3K*, *EIF* protein translation members, *IGF/MTOR*, *IL6-JAK-STAT3*, and *MAPK/p38-MAPK*) (Figure 4D). In contrast, GO analysis of enriched genes in Fos^{GFP-} SCs showed associations with negative regulation of developmental/cellular processes, metabolism, and proliferation (Figure S5E; Table S2). We also compared the transcriptional signatures of Fos^{GFP+} and Fos^{GFP-} fresh SCs with recently published RNA-seq datasets from fresh SCs isolated using standard methods (T3) or from *in-situ*-fixed SCs (T0) prepared using a prefixation protocol aimed at retaining the transcriptional signature of unperturbed, quiescent SCs *in vivo* (Machado et al., 2017). We found a statistically significant overlap between genes enriched in Fos^{GFP+} SCs and those enriched in T3 SCs (overlap of ~50%, $p < 1.0e-21$), whereas Fos^{GFP-} SCs showed significant overlap with T0 SCs (overlap of ~40%, $p = 9.7e-21$) (Figure 4E). All other permutations revealed no statistically significant overlap (Figure S5F).

Several of the enriched pathways in Fos^{GFP+} SCs included members of the MAPK/p38-MAPK family (Figures 4D and 4F). Because p38-MAPK signaling is induced in dormant SCs within 15–20 min after muscle trauma and is essential for transition from quiescence to activation (Jones et al., 2005), we tested whether p38-MAPK signaling acts upstream of FOS. Single fibers from wild-type animals isolated in the presence of the p38 α / β -MAPK inhibitor (p38i, SB202190) showed a 2-fold reduction in PAX7⁺ SCs co-expressing FOS compared with fibers isolated in the presence of vehicle (DMSO) alone (Figures 4G–4I). Thus, the Fos^{GFP+} SC transcriptional signature likely includes upstream activators and downstream targets of FOS/AP-1 as well as other parallel pathways that mediate “early” stem cell activation and muscle repair.

Fos^{CKO} SCs display diminished regenerative activity

To directly test the functional requirement for FOS in SC activation and the response to muscle injury, we established a Cre recombinase (Cre)-LoxP loss-of-function system using *Fos^{fl/fl}*, *ROSA26^{Ai9/+}*, *Pax7^{CreERT2/+}* (Fos-conditional knockout; Fos^{CKO}) and *Fos^{+/+}*; *ROSA26^{Ai9/+}*; *Pax7^{CreERT2/+}* (control) animals. In this system, all *Pax7*-expressing SCs produce the tamoxifen (TAM)-regulated CreERT2. Thus, in the presence of TAM, recombination will occur in SCs at the *Ai9* allele (Madisen et al., 2010), marking them with TdTomato expression, and also at the *Fos* locus, resulting in deletion of exons 2–4 (including the DNA-binding/dimerization domain) and concomitant expression of GFP driven by the endogenous *Fos* promoter (Figures S6A and S6B). TAM administration in Fos^{CKO} mice yielded a high frequency of recombination at the *Ai9* and *Fos* loci, with more than 95% of FACS-analyzed fresh SCs showing expression of TdTomato and GFP (Figure S6C). TAM-treated Fos^{CKO} mice also showed more than 97% reduction of *Fos* mRNA levels in fresh SCs (Figure S6D). As expected, given the lack of expression of *Fos* in quiescent SCs (Machado et al., 2017; van den Brink et al., 2017; van Velthoven et al., 2017; Figures 2D–

2H), induced deletion of *Fos* in *Fos*^{CKO} mice had no effect on SC frequency in unperturbed skeletal muscle (Figure S6E).

To determine whether FOS is needed for SC expansion, we isolated fresh *Fos*^{CKO} and control SCs and cultured them for 7 days, followed by quantification of total Hoechst+ nuclei. *Fos* ablation in SCs resulted in an ~3-fold decrease in the total number of cells, indicating a deficiency of expansion potential in *Fos*^{CKO} SCs (Figure 5A). To directly assess the proliferation kinetics of *Fos*-deleted SCs, we isolated fresh *Fos*^{CKO} and control SCs and cultured each population for 4 or 7 days, with a 3-h pulse of EdU given just before harvest. We observed a nearly 2-fold reduction in EdU+ nuclei among *Fos*^{CKO} compared with control SCs after 4 days in culture but saw no difference in cultures pulsed and analyzed after 7 days (Figure 5B). These results suggest that SCs devoid of *Fos* are likely impaired in their capacity to enter the cell cycle from quiescence but that later cell divisions do not depend solely on FOS activity.

Finally, we evaluated how disruption of FOS activity in SCs affects their capacity to replace and repair damaged skeletal muscle after injury *in vivo*. TAM-treated *Fos*^{CKO} and control animals were subjected to two mechanistically distinct muscle perturbations (cryoinjury or CTX), with muscles harvested for analysis of regeneration at early (7 days) and late (50 days) regenerative time points (Figure 5C). Prior to injury, we detected no differences in the cross-sectional area (CSA) of muscle fibers in *Fos*^{CKO} and control animals (Figures 5D–5F). However, 7 days after cryoinjury or CTX, we observed a defect in muscle regeneration in mice lacking SC expression of *Fos*, with significantly smaller fibers in *Fos*^{CKO} mice (compared with controls), as shown by the mean CSA and distribution of regenerating (centrally nucleated) fibers (Figures 5D, 5G, and 5H; Figures S6G and S6H). The regenerative deficiency in *Fos*^{CKO} mice was even more pronounced 50 days after cryoinjury or CTX injury (Figures 5D and 5I; Figures S6I–S6K). In addition, the pool of Pax7+ SCs failed to fully re-establish by 50 days after injury in *Fos*^{CKO} mice (Figure 5J). These data are consistent with a model where blockade of FOS induction in quiescent SCs impedes rapid entry of these cells into the cell cycle following perceived injury, blunts stem cell expansion in response to myogenic stimuli, and impairs myofiber regeneration and renewal of the SC pool after muscle damage.

***Fos*^{CKO} SCs fail to induce the early-activated pro-regenerative transcriptional program**

To specifically identify FOS-regulated genes (i.e., direct or indirect targets) among the early-activated SC transcriptional signature that may be critical for evoking a rapid SC-mediated repair response, we isolated RNA from fresh *Fos*^{CKO} and control SCs and prepared RNA-seq libraries (Figure 6A). We identified 69 DEGs that were altered 2-fold with an FDR of less than 0.05. 42 genes were enriched and 27 depleted in *Fos*^{CKO} compared with control SCs (Figure 6B; Table S3). *Fos* mRNA was not among the DEGs because of a substantial number of reads mapping to exon 1 that remain intact after CRE recombination and excision of exons 2–4, which encode the DNA binding and dimerization domains of FOS (Figures S6A and S6F). Nonetheless, qPCR validation using primers spanning exons 3–4 confirmed more than 97% depletion of *Fos* mRNA in *Fos*^{CKO} SCs (Figure S6D).

Approximately 33% of the genes depleted in Fos^{CKO} SCs contain a *bona fide* Fos/AP-1 DNA binding motif (5'-TGA G/C TCA-3') within 1 kb upstream of the gene transcription start site (TSS), suggesting direct regulation. In addition, 67% of the genes depleted in Fos^{CKO} SCs were among the enriched genes in fresh Fos^{GFP+} SCs ($p = 1.2e-12$; Figure 6C). Interestingly, FOS-deficient SCs had reduced mRNA levels of the canonical, pro-myogenic factor *Myod* and of *Hmg1* (Figure 6D). GO analysis further revealed that some genes depleted in Fos^{CKO} SCs were associated with muscle cell differentiation and development and with cell motility/migration (Figure 6E; Table S3). However, many of the genes depleted in Fos^{CKO} SCs have not been implicated previously in adult muscle SC biology.

GO term analysis for genes enriched in Fos^{CKO} SCs revealed associations with suppression of cell death (i.e., promoting cell survival), cellular metabolism, gene expression, and cell cycle entry—all properties of quiescent stem cells (Figure 6G; Table S3). These genes included *Sprouty1* (*Spry1*) (Chakkalal et al., 2012; Shea et al., 2010), the Notch effector *HeyL* (Bjornson et al., 2012; Figure 6F), and a multitude of other known cell cycle inhibitors, including *Cdkn1c*, *Gas1*, *Btg1*, *Cul3*, *Bhlhe40*, *Ddit3*, and *Jdp2* (Jun dimerizing protein 2), a potent inhibitor of Jun/ AP-1 activity. In addition, some genes enriched in Fos^{CKO} SCs overlapped with genes enriched in the Fos^{GFP-} subset (3 of 42, $p = 0.032$), although there was also overlap with genes shared among the Fos^{GFP+} SCs (14 of 42, $p = 1.3e-5$; Figure 6C; Table S3). These results indicate that abrogation of FOS activity in early-activated SCs results in retention of gene transcripts that enforce cellular quiescence and in depressed expression of a select cohort of secondary response genes, many with unrecognized and potentially crucial roles in early SC regenerative biology.

Art1 is a direct FOS target whose pharmacological and genetic disruption impairs SC function

We hypothesized that genes depleted in Fos^{CKO} SCs may serve as very early activation effectors that are essential for rapidly converting quiescent SCs into fully activated stem/progenitor cells. To test this hypothesis, we prioritized one of the most depleted genes in fresh Fos^{CKO} SCs, *Art1* (Table S3); the effects of the Nicotinamide Adenine Dinucleotide(NAD)-consuming post-translational modification (PTM) MARYlation, catalyzed by ART1, remain poorly understood in any adult stem cell process. *Art1* is likely a direct FOS target gene, given that its early-induced mRNA levels are dependent on FOS activity in SCs (Figure 7A) and because chromatin immunoprecipitation studies reveal FOS binding near a canonical FOS/AP-1 motif ~700 bases upstream of the *Art1* TSS in cultured SCs ectopically expressing FOS (Figure 7B). Furthermore, RNA expression analysis showed that, although *Art1* mRNA is induced in SCs as a consequence of muscle damage (e.g., during the SC isolation procedure; Figure 7C), its rapid downregulation (relative to fresh SCs) in proliferating SCs on day 7 in culture (Figure 7D) mirrors the kinetics of FOS induction. *Art1* mRNA is upregulated again in differentiating myoblasts as they transition into mature myotubes (Figure S7A), consistent with a prior report (Friedrich et al., 2008). These data suggest that ART1, like FOS, may mediate the very early transition of quiescent SCs to the activated stem cell state.

To discern whether MARYlation, the PTM catalyzed by *Art1*, is necessary for cell cycle entry from quiescence and stem/progenitor cell expansion, we sorted fresh SCs into wells containing GM supplemented with vehicle or meta-iodobenzyl-guanidine (MIBG), a rapid inhibitor of global mono-ADP-ribosylase activity (Loesberg et al., 1990). Strikingly, we found a considerable deceleration in cell cycle entry kinetics (~2-fold decline in EdU+ nuclei detected after a 3-h EdU pulse) 3 days later (Figure 7E) and a dose-dependent suppression of progenitor cell expansion starting on day 2 and persisting until day 6 in cultures supplemented with MIBG (relative to vehicle) (Figures S7B–S7D). Confirming these results, lentiviral delivery of two different *Art1*-targeting short-hairpin RNAs (shRNAs) to fresh SCs immediately after their isolation caused a similar decrease in cell cycle entry and blunted SC expansion compared with a non-targeting shRNA control (Figure 7F; Figure S7E). We also observed a reduction in cell membrane-localized ADP ribosylation in MIBG-treated, Fos^{CKO}, and sh*Art1*-targeted SCs relative to controls on day 3 in culture (Figure 7G; Figure S7F), confirming the known activity of MIBG as a MARYlation inhibitor and consistent with a requirement for FOS and ART1 activity for driving cell-surface ADP ribosylation events in early-activated SCs.

Lastly, to interrogate the role of MARYlation in directing SC repair responses *in vivo*, we injured TA muscles of wild-type mice with CTX (day 0), and 12 h later injected MIBG or vehicle into the injured muscles once a day for 2 consecutive days (i.e., coincident with the G₀-S phase transition of SCs in injured muscle; Rodgers et al., 2014; Figure 7H). We then quantified the abundance of Pax7+ SCs and the CSA of regenerating muscle fibers at 7 days post injury (dpi) in both groups. Interestingly, we found an approximate 2-fold decrease in the content of Pax7+ SCs and a significant decrease in the CSA of regenerating myofibers at 7 dpi in muscles injected with MIBG (Figures 7I–7L). These findings reveal a role for *Art1* and NAD(+)-dependent MARYlation as critical inducers of the highly regenerative stem cell program, whose expression is triggered by the FOS-induced early-activation gene network in muscle SCs.

DISCUSSION

Enduring mysteries regarding the basic molecular and cellular mechanisms by which quiescent stem cell populations are initially turned on (activated) in response to tissue damage and subsequently programmed for regenerative functions remain a major roadblock for the therapeutic manipulation of these cells for regenerative medicine. This study provides missing resolution into the very early events in adult stem cell activation, using skeletal muscle as a model system.

Our work recapitulates a defining feature of FOS/AP-1: its rapid (within hours) and transient induction in cells upon exposure to external stimuli (Greenberg and Ziff, 1984). In our study, FOS was immediately and transiently induced (within 1.5 h of injury) in SCs in response to muscle perturbation, including chemical/mechanical dissociation coupled with (1) FACS-based purification, (2) isolation of intact single muscle fibers, and, most importantly, (3) chemically induced muscle trauma *in vivo*. Interestingly, the observation that FOS is induced in a sub-fraction of SCs as a consequence of muscle damage suggests that previously recognized molecular and functional heterogeneity within the SC pool may be influenced,

in part, by proximity to local stress signals released by damaged muscle fibers and/or blood vessels. In such a model, SCs closer to the site of injury *in vivo* or more exposed to chemical and mechanical stress during *ex vivo* isolation may induce FOS to higher levels via upstream p38-MAPK activation and therefore exhibit increased propensity to exit quiescence (Jones et al., 2005). Future studies are required to conclusively discern whether FOS is expressed in all SCs but with different dynamics and regulation or whether it may be uniquely expressed by a subset of the SC pool in response to muscle damage (Figure S5G).

Using a Fos^{GFP} reporter mouse (expressing a Fos^{GFP} fusion protein), we demonstrated that the subset of fresh SCs marked by FOS^{GFP} expression at the time of isolation displays enhanced regenerative properties, including rapid entry into the cell cycle from quiescence, higher clonal expansion potential, and more efficient engraftment into skeletal muscle. Thus, although it has been a long-standing view in the field that SCs perceived to be “more quiescent” have higher regenerative capabilities, including engraftment into skeletal muscle (Chakkalakal et al., 2014; Kuang et al., 2007; Rocheteau et al., 2012), our results indicate that the ability of a quiescent SC to rapidly activate from dormancy may be the most direct positive predictor of its future regenerative performance. This notion is consistent with a recent study showing that highly regenerative label-retaining cells (LRCs), thought to represent a deeply quiescent “reserve” SC subset, appear to activate from quiescence at a faster rate compared with their less functional non-LRC counterparts (Chakkalakal et al., 2012; Kimmel et al., 2020).

To evaluate whether FOS expression simply marks SC activation or is functionally required for efficient muscle repair, we employed a loss-of-function model to eliminate FOS from early-activated SCs. Interestingly, we found that FOS accelerates the transition of SCs from quiescence to activation, a ratelimiting step in muscle repair that typically requires 2–3 days (Rodgers et al., 2014). However, when cells accomplish this transition (i.e., in actively proliferating progenitor cells), absence of FOS has no apparent effect on the rate of future cell divisions, suggesting potential compensation by other AP-1 family members or parallel pathways (Brown et al., 1998). Nonetheless, delaying initial entry of SCs into the cell cycle as a consequence of FOS ablation reduced the total number of stem/progenitor cells that expanded upon exposure to myogenic stimuli, leading to incomplete muscle repair and failure to effectively maintain the Pax7+ SC pool even 50 days after muscle trauma. These results implicate FOS as a critical mediator of stem cell activation whose rapid and transient activity in SCs has a long-lasting effect on the behavior of these cells and the robustness of muscle repair.

The function of FOS as a transcriptional regulator in early-activated SCs also provided us with a unique molecular lever for discovering previously hidden pro-repair genes involved in the earliest steps of muscle regeneration. Indeed, analysis of the unique set of FOS-regulated target genes in SCs uncovered a pathway involving NAD(+)/ART1/MARylation that boosts muscle repair by accelerating the rate of SC entry into the cell cycle, expanding the pool of myogenic cells and facilitating efficient muscle repair. Our future work will focus on identifying the molecular targets and downstream signaling networks of ART1 activity in SCs that drive the muscle repair program.

Art1 is a cell-membrane-bound, glycosylphosphatidylinositol (GPI)-anchored enzyme that catalyzes the transfer of a single ADP-ribose molecule from NAD(+) to arginine residues of protein substrates (Cohen and Chang, 2018). Although *Art1* is expressed in differentiating myoblasts as they fuse to form myotubes and in myofibers *in vivo* (Friedrich et al., 2008; Leutert et al., 2018), we report that *Art1* is first induced in SCs via FOS/AP-1 during the early response to muscle trauma. Like Fos and NAD(+) (Ryall et al., 2015), *Art1* is transiently present in activated SCs, and its mRNA levels substantially decline by the time these cells are actively proliferating. Although it is still unclear why muscle trauma induces only transient ART1 activity in SCs, recent work showing that ART1 over-activation can promote lung and colon cancer (Xu et al., 2017) raises the possibility that timelimited ART1 activity protects against uncontrolled and potentially tumorigenic proliferation. On the other hand, failure of ART1-mediated MARYlation may be linked to stem cell and tissue dysfunction associated with aging and disease. For example, cellular NAD(+) levels decline with age and in muscular dystrophy (Ryu et al., 2016), and boosting cellular NAD(+) levels has been reported to enhance stem cell-mediated repair in the skeletal muscle, brain, gut, and blood of older mice (Igarashi et al., 2019; Vannini et al., 2019; Zhang et al., 2016). Of course, systemic elevation of NAD(+) can act as a co-factor for many different enzymes, including Sirtuins, Poly(ADP-Ribose) Polymerases (PARPs), and ART family members, and so further work is needed to clarify the relative contribution of ART1-mediated MARYlation to this particular biological phenomenon.

In conclusion, we report an “early” activation pathway in adult muscle stem cells that is initiated by the AP-1 TF FOS but ultimately executed by a network of “pro-regenerative” downstream target genes, including *Art1*, whose collective activities synergize to instruct essential stem cell functions (i.e., division, migration, and differentiation). We suspect that the FOS-induced early activation response is a conserved feature of other adult tissue-specific stem cells because we detected Fos^{GFP+} cells in other stem cell compartments, including Sca1+ fibro-adipogenic progenitor cells (data not shown). Given the general interest in harnessing adult and other types of stem cells for regenerative medicine, we propose that identifying FOS-mediated early activation targets in other clinically relevant stem cells may pave the way for new strategies to enhance tissue and organ regeneration (Shelton et al., 2019).

STAR★METHODS

Detailed methods are provided in the online version of this paper and include the following:

RESOURCE AVAILABILITY

Lead contact—Further information and requests for resources and reagents should be directed to and will be fulfilled by the Lead Contact, Amy J. Wagers (amy_wagers@harvard.edu)

Materials availability—This data did not generate any unique reagents

Data and code availability—The Microarray and RNA-Seq data generated in this study were deposited in the Gene Expression Omnibus (GEO) database:GSE119695 and

GSE119895. Previously published Microarray and RNA-Seq data used in this study can be accessed under GEO:GSE47177, GSE64379, and GSE103163 and ENA:PRJEB10091 codes. Additional unprocessed data has been deposited to Mendeley Data (<https://doi.org/10.17632/hng8s6x47h.1>).

EXPERIMENTAL MODEL AND SUBJECT DETAILS

Generation of *Fos^{fl/fl}*; *ROSA26^{Ai9/+}*; *Pax7^{CreERT2/+}* (*Fos^{cKO}*) and *Fos^{+/+}*; *ROSA26^{Ai9/+}*; *Pax7^{CreERT2/+}* (control)—The Harvard University Institutional Animal Care and Use Committee (IACUC) approved all animal protocols used in this study. Homozygous *Fos^{fl/fl}* (C57BL/6J) mice (Fleischmann et al., 2003) were obtained from M. Greenberg at Harvard Medical School (HMS), and backcrossed to C57BL/6J (Jackson Labs) mice for 3 generations. Resulting *Fos^{fl/fl}* animals were crossed with *Pax7^{CreERT2/CreERT2}* animals (C57BL/6J), and F1/F2 animals were crossed accordingly to generate *Fos^{fl/fl}*; *Pax7^{CreERT2/CreERT2}* (breeder parent 1, for generating *Fos^{cKO}* animals). Breeder parent 1 was maintained by crossing *Fos^{fl/fl}*; *Pax7^{CreERT2/CreERT2}* animals. To generate *Fos^{fl/+}*; *ROSA26^{Ai9+/Ai9+}* (breeder parent 2, for generating *Fos^{cKO}* animals), *Fos^{fl/fl}* animals were crossed to *ROSA26^{Ai9/Ai9}*, and resulting F1/F2 animals were mated accordingly. To maintain breeder parent 2 (for generating *Fos^{cKO}* animals), *Fos^{fl/fl}*; *ROSA26^{Ai9+/Ai9+}* animals were crossed with *Fos^{fl/+}*; *ROSA26^{Ai9+/Ai9}* To generate *Fos^{fl/fl}*; *ROSA26^{Ai9/+}*; *Pax7^{CreERT2/+}* (*Fos^{cKO}*) animals, *Fos^{fl/fl}*; *Pax7^{CreERT2/CreERT2}* animals were bred with *Fos^{fl/+}*; *ROSA26^{Ai9+/Ai9+}*. To generate *Fos^{+/+}*; *ROSA26^{Ai9/+}*; *Pax7^{CreERT2/+}* (control) animals, *Pax7^{CreERT2/CreERT2}* animals were crossed with *ROSA26^{Ai9+/Ai9+}*. To maintain breeder pairs for control animals, *Pax7^{CreERT2/CreERT2}* and *ROSA26^{Ai9+/Ai9+}* were intercrossed in house. All *Fos^{cKO}* and control animals, as well as breeders, were housed on adjacent racks in the animal facility and handled with identical downstream procedures. Cohorts of adult control and *Fos^{cKO}* mice used for a given experiment often included mice from multiple litters and were between the ages of 4–10 months. Adult mice for each genotype were age-matched (no more than 3 weeks difference in ages) and sex-matched for each experiment. Both male and female mice were used.

Additional mouse strains—C57BL/6J, C57BL/10ScSn-*Dmd^{mdx}/J*, B6.Cg-Tg(*Fos/EGFP*)1–3Brth/J, and C57BL/Ka- β -actin-EGFP mice were handled, housed, and matched by age and sex as described above. Animals from multiple litters were frequently used in a given experiment. Male and female mice ranging from 3–6 months of age were used for these strains.

METHOD DETAILS

Tamoxifen (TAM) administration—TAM was dissolved in corn oil at a concentration of 20 mg/mL by continuous rotation at 37°C O/N, stored at 4°C, and used within 1 week. *Fos^{cKO}* and control animals were given 5-consecutive Intraperitoneal (IP) injections of 75 mg/kg of body weight, followed by 2 days of rest, then switched to standard diet supplemented with TAM (Envigo, 500 mg/kg diet) for roughly 4–12 weeks, with the duration on TAM diet depending on the experimental endpoint.

Satellite cell isolations by FACS—Fresh muscle SCs were isolated as previously described (Maesner et al., 2016). Briefly, hind-limb, abdominal, and tricep muscles were isolated from animals and digested in Enzyme Mix 1, containing 0.2% collagenase type II (285 U/mg) in Dulbecco's modified eagle medium (DMEM), for 90 minutes in a 37°C shaking incubator. The enzyme activity was inactivated by carefully washing the digested muscle with 20% Fetal Bovine Serum (FBS) in F10 medium, followed by two sequential washing steps with Phosphate Buffered Saline (PBS). Single fibers were liberated from digested muscle by gentle trituration and enriched through 3 gravitational sedimentation steps for 20, 15, and 10 minutes at 37°C, where after each time-point, supernatant (containing low density blood cells) was removed and replaced with fresh PBS. After the final sedimentation step, enriched single fibers were digested in Enzyme Mix 2, containing 0.0125% Collagenase type II/0.05% Dispase (1.81U/mg) in F10, for 30 minutes at 37°C to dissociate mono-nuclear cells from individual muscle fibers. Cell suspension containing Enzyme Mix 2 was inactivated with 2 mL of FBS, pipetted 10 times, lightly spun (~500 rpm) to remove cellular debris, and then filtered through a 70-micron cell strainer. Resulting cells were resuspended in staining media (2% FBS in Hanks Balanced Salt Solution (HBSS), SM), counted, and then incubated on ice for 30 minutes with fluorescently-conjugated antibodies to detect the following antigens: anti-Ly6A/E-APC or anti-Ly6A/E-PE (Sca-1) (1:200), anti-CD31APC (1:200), anti-CD45-APC (1:200), CD11b-APC (Mac-1) (1:200), CD29-APC-Cy7 (β 1-Integrin) (1:200), CD184-Biotin (CXCR4) (1:100). A secondary antibody, Streptavidin-PeCy7 (1:200) for CXCR4 detection, was incubated with the appropriate samples on ice for 20 minutes, followed by two sequential wash steps with. Stained cells were analyzed by FACS using the BD FACSAria III cell sorter. Single color controls and FMOs were prepared for all experiments (i.e., No templated single-color controls or FMOs were used). After gating on physical parameters and live cells (Propidium Iodide-negative/Calcein Blue-positive) (Maesner et al., 2016), Satellite Cells were defined as the Sca1⁻; CD45⁻; CD11b⁻; Ter119⁻; CD31⁻; CD29⁺ (β 1-Integrin); CD184⁺ (CXCR4) cell population. The population of satellite cells positively selected for β 1-Integrin and CXCR4 expression overlaps significantly (> 90%) with satellite cells isolated using other positive-selecting antigens, including VCAM1 and α 7-integrin/CD34 (Maesner et al., 2016). We require approximately 8–10 hours to transition from mice (n = 3–6 mice) to antibody-stained, mononuclear cells ready for FACS. Since we typically double-sort our satellite cell populations, an additional 2–4 hours is required before cells are ready for subsequent experimentation.

Gating strategy for GFP- and GFP+ Fresh SCs in Fos^{GFP} animals—Using Fluorescent Minus One (FMO) controls (cells from age- and sex-matched WT mice), we set our GFP- gate such that it contains over 90% of the cells, while the GFP+ gate is typically set to include no more than ~2% false positives. Under these parameters, we find approximately 15%–25% of the Sca1⁻; CD45⁻; CD11b⁻; Ter119⁻; CD31⁻; CD29⁺ (β 1-Integrin); CD184⁺ (CXCR4) Satellite Cells in the GFP- gate and roughly 50%–60% in the GFP+ gate. Each experiment included new single-color controls and FMOs for fluorophore compensations and gating of GFP+ cells, respectively, as this ensures more accurate and consistent results than the use of templated compensations and controls from previous days.

Primary cell culture—Fresh Satellite Cells were double-sorted into pre-coated, 96-well plates containing standard Growth Media (GM). Plates were pre-coated for 24 hours with a coating media containing Collagen Type 1 (1ug/ml final) and Laminin (10 ug/ml) in PBS. GM consists of 20% Donor Horse Serum (DHS), 1% Penicillin/Streptomycin, and 1% GlutaMax in F10 media, with daily addition of 5 ng/mL of bFGF. GM was changed every 48 hours by removing ½ volume and adding in Fresh GM 3 consecutive times. Satellite cell progeny cultured longer than 1 week were passaged by removing ½ GM and adding back the same volume of 5 mM EDTA (to achieve a 2.5 mM final concentration), incubated for 20 minutes at 37°C to allow cell detachment, centrifuged at 1200 RPM to pellet cells, resuspended in fresh GM, counted, and seeded to new wells at desired densities.

Ex vivo proliferation assays—Satellite Cell expansion was quantified by fixing the cell cultures in 4% PFA for 15 minutes, washing 3× with PBS, staining the nuclei with Hoechst dye, and counting the total Hoechst-positive nuclei using the Celigo high-throughput imaging platform software. For measuring cell cycling kinetics directly, EdU (10 µM) was pulsed for 3 hours in the cultures, and then samples were processed according to the manufacturer's protocol (Click-IT EdU Alexa Fluor 647 Imaging Kit). Roughly 80% of the wells were imaged and stitched using the Zeiss Cell Discoverer 7 High-Throughput Imaging system, and EdU+ nuclei among all scored Hoechst+ nuclei (> 1500 Hoechst+ nuclei per replicate per condition) within the stitched images were quantified using ImageJ (FIJI) software.

Ex vivo differentiation assays—Fresh Satellite Cells were grown for 5 days in GM with daily addition of bFGF (5 ng/mL), harvested using 2.5 mM EDTA (as described above), counted, and seeded at 4000 cells per 96-well in GM without bFGF. The following morning, the media was changed to differentiation media (DM), consisting of 2.5% Donor Horse Serum and 1% Penn/Step in DMEM. We define differentiating/committed myoblasts and terminal myotubes as those cultures after 24 hours (as slightly elongated myoblasts with no fusion) and 72 hours (fully formed multi-nucleated, myotubes) in DM, respectively.

Single fiber isolation—Skeletal muscle single myofibers were isolated as described previously (Bentzinger et al., 2013; Pasut et al., 2013). Enumeration of > 100 satellite cells (on average) was conducted across a minimum of 30 fibers per replicate for either condition (Pre-Fix/No Pre-Fix at t0, Vehicle/p38i). For Pre-Fix conditions, Extensor Digitorum Longus (EDL) muscle was dissected and immediately fixed in 0.5% PFA for 10 minutes prior to collagenase dissociation (0.2%) for 2 hours at 37°C. The resulting digested EDL muscle was subsequently triturated to generate single fibers. For the p38 studies, EDL muscles were incubated with a p38 inhibitor (SB202190, Sigma) at a concentration of 10 µM or vehicle during the dissociation process with collagenase (0.2%) for 2 hours at 37°C, and p38i or vehicle was present in the subsequent washing steps. All liberated fibers were then fixed with 4% PFA for 10 minutes prior to antibody staining. Anti-PAX7 antibody (DSHB, supernatant) was used at a dilution of 1:200. Anti-FOS antibody (Abcam, ab190289) was used at a dilution of 1:1500.

Histology and processing of skeletal muscle samples—Tibialis Anterior (TA) or Tibialis Anterior/Extensor Digitorum Longus (TA/EDL) muscles were isolated from mice, embedded in O.C.T., and rapidly frozen in isopentane cooled with liquid nitrogen for approximately 1 minute. Frozen TA muscles were then stored at -80°C , for at least two days, before the muscle was cryo-sectioned at 8–12 depths spanning the middle two-thirds of the muscle (mid-belly) with a $12\ \mu\text{m}$ thickness per section. Fresh frozen tissue sections were then used for Hematoxylin and Eosin (H&E) staining to evaluate the cross-sectional area (CSA) of regenerating (centrally-nucleated) skeletal muscle or to quantify the total number of muscle fibers per section, or used for immunohistochemical staining (IHC) for FOS, PAX7, and DYSTROPHIN detection.

Immunofluorescence (IF) and immunohistochemistry (IHC)—IF for FOS and MYOD in cultured cells was performed by fixing cells with 4% PFA for 15 minutes followed by 3×5 -minute washes in PBST (0.1% Tween in PBS). Cells were permeabilized with 0.3% Triton-X in PBS for 20 minutes, followed by 3×5 -minute washes in PBST. Cells were then incubated for 2 hours at room temperature (RT) in blocking buffer (3% Bovine Serum Albumin (BSA), 5% Normal Goat Serum (NGS), 8% Protein Concentrate (Vector Labs, MOM-Immuno-Detection Kit), and 0.1% Triton-X in PBS). Without washing, primary antibody (1:1000 for anti-FOS (sc7202), 1:1000 for anti-MYOD (5.8A)) was added to a fresh batch of blocking buffer that was incubated with cells O/N at 4C, and the following morning plates were washed 4×5 minutes in PBST. Secondary antibody (1:250, see reagents list) was added to 3% BSA in PBST and incubated with cells for 1 hour at RT. Lastly, cells were washed for 4×15 minutes in PBST, and Hoechst dye was added into the final wash step for nuclei detection. Roughly 80% of the wells were imaged and stitched using the Zeiss Cell Discoverer high-throughput imaging platform, and subsequently quantified in ImageJ (FIJI). For MYOD protein quantification in 6-hour cultured SCs, > 300 Hoechst+ nuclei were scored for Fos^{GFP+} and Fos^{GFP-} SC cultures.

For ADP-Ribose IF, we performed the protocol described above with the following modifications. First, we used PBS (instead of PBST) for each wash step and buffer, and completely omitted the cell permeabilization step. We also used a primary antibody detecting mono- and poly-ADP Ribose (Cell Signaling Technologies, E6F6A, 1:500). After ~3 days of culture, wells were imaged on a Zeiss LSM 880. Multiple 20X images were taken per well (~6–12 unique fields)—in a blind manner using coded plates and by choosing the field of view in the blue channel only (hoechst+ cells)—and then quantifying cell surface MARYlation (green channel) for each cell in the field using ImageJ (Fiji). To obtain a background-corrected total cell fluorescent value for each cell, we determined the total integrated signal for a Region of Interest (ROI) (i.e., SCs showing positive signal for cell surface ADP Ribosylation) and subtracted that value from the total fluorescent integrated signal of an equally sized ROI in a neighboring location with no signal. These values were then divided by 10 and plotted with GraphPad Prism 7.

For immuno-histochemical (IHC) staining for PAX7, FOS, and DYSTROPHIN, fresh frozen TA muscle sections of $12\ \mu\text{m}$ thickness were prepared as discussed above. Each section was lightly fixed with 2% PFA for 5 minutes at RT, washed for 3×5 minutes in PBST, incubated with 0.1M Glycine (to quench the fixation reaction), and washed again for 3×5 minutes in

PBST. Sections were then permeabilized with 0.3% Triton-X in PBS for 20 minutes, and subsequently washed in PBST for 3× 5 minutes. For PAX7 staining (anti-mouse PAX7), sections were initially incubated with 10% MOM reagent (Vector Labs, MOM-Kit) in PBST for 30 minutes at RT. This step ensures that IgG in the mouse tissue section is blocked prior to the addition of primary (anti-mouse) and secondary (goat anti-mouse) antibodies. Without washing, sections were then incubated with blocking buffer (3% BSA, 5% NGS, 8% Protein Concentrate (Vector Labs, MOM-Kit), and 0.1% Triton-X in PBS) for 2 hours at RT. For PAX7 staining, 1% MOM reagent was included in the blocking buffer.

Without washing, primary antibody (1:1500 for α -FOS (ab190289), 15 μ g/ml for α -PAX7 (DSHB, concentrate)/1:2 of PAX7 Supernatant (DSHB), 1:50 for α -DYSTROPHIN (ab15277)) in 3% BSA and 8% protein concentrate (Vector labs) was incubated with sections O/N at 4°C, and the following morning sections were washed 4× 15 minutes in PBST. Secondary antibody (see reagents list) was added to 3% BSA in PBST and incubated with sections for 1 hour at RT, and then washed for 4× 15 minutes in PBST. For PAX7 staining, we use an anti-mouse IgG1-specific antibody (see reagents list). Following washes, sections were mounted and stained with DAPI (Vectashield), and imaged on a Zeiss 880 Inverted microscope. For PAX7 immuno-staining in regenerating muscles (7dpi) we made several modifications. First, we performed an antigen retrieval by boiling muscle sections in Citrate Buffer (pH 6.8) for 15 minutes, followed by two sequential washes in DI water, and then proceeded to the permeabilization step. Second, after permeabilization, instead of blocking mouse IgG with MOM reagent, we blocked with 10% Affinipure Fab Fragment goat anti-mouse IgG (H+L) in PBST for 1 hour instead, and then carried on with our standard IHC protocol as described above.

For the quantification of PAX7+FOS+ satellite cells before and after skeletal muscle injury (CTX, 10 μ M), we report values from one muscle section located at the mid-belly of the TA/EDL (i.e., site of CTX injection) for each replicate of each time-point (all muscles compared were of equal sizes). Greater than 300, 100, and 60 total PAX7+ SCs were scored for T0, T1.5, and T12 hour, respectively. For the quantification of total PAX7+ SCs per TA/EDL muscle section, each data point represents an average of ~3 depths from the mid-belly of the muscle for each replicate for each condition. Whole muscle sections were imaged using a Zeiss LSM 880 and the resulting images were exported to ImageJ for manual quantification.

Lentivirus production and infection of Fresh SCs—For producing virus that express control or *Art1*-targeting shRNAs, 293T cells were seeded at 400,000 cells per 10 cm dish and cultured in DMEM with 10% FBS for 24 hours prior to transfection. In brief, 9 μ g of packaging plasmid (psPAX2), 0.9 mg of envelope plasmid (pMD2.G), and 9 mg of pLKO-Non-Targeting-shControl (NTC) or pLKO-sh*Art1_1*, or pLKO-sh*Art1_2* was transfected (MIRUS TransIT transfection reagent) into 293T cells according to the manufacturer's protocol and incubated at 37°C. For producing virus that ectopically express FOS or GFP cDNAs in a Doxycycline (DOX)-inducible manner, Fos and eGFP cDNAs were cloned at the MCS (i.e., NotI and KpnI sites) of the entry vector, pEN_TTmcs, and then recombined into the pSLIK-Hygro destination vector using Gateways LR Clonase II kit according to the manufacturer's protocol. All plasmids were sequence verified. 293T cells were seeded

at 400,000 cells per 10 cm dish and cultured in DMEM with 10% FBS for 24 hours prior to transfection. In brief, 10 µg of pSLIK plasmid, 7.5 µg of each packaging plasmids pMDLg/pRRE and pRSVREV, and 5 mg VSV-G envelope plasmid were co-transfected (Lipofectamine 2000, Invitrogen) into 293T cells according to the manufacturer's protocol.

Viral supernatant was collected 72 hours after transfection, concentrated using Lenti-X concentrator reagent, resuspended in 200 µL's of myogenic Growth Media (GM) supplemented with 10 mM HEPES buffer (virus mix), and aliquoted and stored at -80°C. Virus was tested to determine the least toxic amount (1/300–350 dilution) that infected the most cultured stem/progenitor cells as determined by Puromycin (shRNA expression) or Hygromycin (cDNA expression) selection for 2 or 5 days, respectively. Fresh SCs were sorted into 96-well plates with half the typical GM media (100 µL), and within 1 hour, 100 µL of a viral-media mix (consisting of 1/300–350 amount of virus and 8 µg/mL of Polybrene in GM) was added to each well of a 96-well plate, the plate was covered with parafilm and incubated at 37°C for 15 minutes, and then subsequently spun at 2000 RPM in a Beckman Coulter Allegra 6KR at 32°C for 1.5 hours. After 1.5 hours, virus was removed from the wells by extracting 100 µL of viral-media mix and adding back 100 µL of fresh GM 8 times. Fresh bFGF was added daily to the cultures.

Chromatin immunoprecipitation quantitative PCR (ChIP-PCR)—3000 Fresh SCs in 96-well plates were infected (1:300) with virus expressing a Fos or GFP cDNA one day after their isolation, selected with 100 µg/ml of Hygromycin for 5 days, and then expanded for 2–3 weeks in GM to obtain roughly 10× 15-cm plates for each of the following conditions: (1) pSLIK-FOS with doxycycline, (2) pSLIK-FOS without doxycycline, (3) pSLIK-GFP with doxycycline, and (4) pSLIK-GFP without doxycycline. Doxycycline (1 µg/ml) was added to the media 24 hours prior to harvesting cells. Immediately after the 24-hour time-point, media was removed from each plate and washed once with dPBS, and then 12.5 mL's of crosslinking buffer (10mM HEPES-NaOH pH7.5, 100mM NaCl, 1mM EDTA, 1mM EGTA) with 1% formaldehyde was added to each plate, immediately followed by rocking for 10 minutes at room temperature. A final concentration of 0.11M Glycine was added to each plate to stop the fixation reaction. Next, fixed cells from each condition were scrapped from the plates in dPBS on ice, combined, spun down at 500 g for 5 minutes and the cell pellet was stored at -80C for a maximum of 4 weeks. We performed lysis, sonication, and antibody-bead coupling, immunoprecipitation, and elution as directed in the Diagenode iDeal ChIP-qPCR kit. Reaction volumes are calibrated according to the number of cells harvested. Briefly, sonication was done for 35 cycles of 30 s off and then 30 s on at the high setting of the Diagenode Bioruptor. For each IP reaction, ~20 µg of sheared chromatin is incubated overnight at 4°C with 30 µL of Protein A-coated magnetic beads coupled with 1 µg of anti-Fos antibody (Gift from M. Greenberg) or 1 µg of anti-IgG antibody. The elution is done in 100 µL DIB buffer from the kit and the DNA is stored at -20°C. In parallel, 1% of the DNA volume from each sample input is eluted and stored at -20°C. 5 *ArtI*-specific primers were designed to flank the canonical AP-1 site ~700 bases upstream of the *ArtI* TSS, and several quality control experiments were performed to confirm specificity (i.e., single band) and efficient priming in qPCR studies. qPCR reactions including 1 µL of eluted IP'ed DNA or eluted 1% input along with water and SYBR Green

master mix reagent (according to manufacturer's protocol) was run on a QuantStudio 6 Flex (Thermo Fisher) RT-PCR machine, for 1 cycle of 95°C for 10 minutes, and then 40 cycles of 95°C for 10 s and 60°C for 30 s, followed by a standard melting curve cycle. The percent input of enrichment was defined by the following formula: $100 * 2^{(Ct_{input} - \log_2(100)) - Ct_{IP}}$. Note: the magnitude of FOS binding (i.e., Fold enrichment) at the Art1 promoter (relative to IgG controls) is influenced by how differentiated (ratio of round to more elongated cells) the myogenic cultures were at the start of doxycycline addition. To ensure that more round stem/progenitor cells are the predominant population in the expanding cultures one must change media every 48 hours and never allow the confluency to reach greater than 70%.

MIBG administration to Fresh SCs *ex vivo* and direct injection into TA muscles

in vivo—Fresh MIBG (25 mg) was dissolved into 1 mL of MeOH to give a stock solution at a concentration of 77,140 μ M and stored at 4°C for a maximum of 1–2 weeks. Longer storage times not recommended due to rapid evaporation of MeOH. Stock solution of 77,140 μ M MIBG was serially diluted in MeOH to 15,428 μ M and 1,543 μ M, and 3.24 μ Ls of methanol (i.e., for vehicle) or each dilution of MIBG was independently added to 4,997.76 μ Ls of Growth Media (GM) giving a final volume of 5,000 μ Ls at a concentration of vehicle (0.06% Methanol), 50, 10, and 1 μ M of MIBG-supplemented GM or Saline, respectively. Freshly isolated Satellite Cells were sorted directly into 96-well plates containing GM supplemented with vehicle (0.06% MeOH) or 1, 10, or 50 μ M MIBG. Fresh MIBG or vehicle-supplemented GM (including 5 ng/ml of bFGF) was added to each well daily by removing $\frac{1}{2}$ media and then adding back $\frac{1}{2}$ media 3 consecutive times. For *in vivo* injections, 30 μ Ls of 50 μ M MIBG or vehicle (0.06% MeOH) in Saline solution was injected directly into the TA muscle for two consecutive days (one injection per day) after a CTX injury (50 μ Ls of 10 μ M), followed by the harvesting of regenerating TA/EDLs 7 days after the initial injury.

***In vivo* regeneration assays**—Cardiotoxin (CTX) injury for *in vivo* regeneration studies were performed by injecting 50 μ Ls of 10 μ M CTX (Latoxan) into the TA muscle of animals. Freeze injuries were conducted by opening up the skin to expose the TA muscle, and firmly pressing a freezing flat metal rod (cooled in dry-ice) to the muscle for at least 15 s. After monitoring animals for 7 days, mice were euthanized and regenerating TA/EDL muscles were harvested and sectioned throughout the muscle at 8–10 depths centered at the mid-belly (each depth separated by roughly 200 microns). Histology slides were coded to ensure that the analyzer of the sections was blind to the identity of each slide. For each slide containing sections from 8–10 depths, the section giving rise to the greatest number of centrally nucleated fibers that was closest to the injury (i.e., breakdown of muscle architecture) was used for Cross Sectional Area (CSA) analysis. Four to five representative 20X-magnified images surrounding the most injured areas within the section were used for quantification. In total, the CSA of 1000–5000 fibers per genotype per condition are reported. CSA of regenerating fibers were analyzed using Zeiss imaging software or ImageJ (Fiji) and CSA values for each sample were exported to excel and unmasked to complete the analysis. For quantifying the total number of muscle fibers per section, sections were H&E-stained, imaged using a Zeiss Axioscan.Z1, and then exported into ImageJ (Fiji)

for manual quantification. Each data point represents the average of ~3 depths from the mid-belly of the TA muscle.

Cell transplantation—Recipient *Mdx* (C57BL/10ScSn-Dmd^{mdx}/J) mice were pre-injured by injecting 25 μ L of Cardiotoxin (CTX, 10 μ M) into the TA muscle 24 hours prior to cell transplantation. The following day, 3000 Fos^{GFP+} and 3000 Fos^{GFP-} donor Fresh SCs were re-suspended in 20 μ L of staining media (2% FBS in HBSS) and injected (BD Biosciences insulin syringes, 31 gauge) into the contralateral TAs of recipient mice. Three weeks after injection, TA/EDL muscles were explanted, sectioned throughout the muscle at 10–12 depths (separated by roughly 200 microns) centered at the mid-belly, and then stained for DYSTROPHIN (see above for staining protocol). Each data point represents the total number of Dystrophin+ fibers that were averaged from 3 depths from the mid-belly of the TA/EDL muscle.

Protein analysis with Wes (ProteinSimple)—10,000 Fresh Satellite cells were directly sorted into 96-well plates containing 5 μ Ls of RIPA protein lysis buffer, and samples were processed according to the manufacturer's protocol. Antibodies, sample protein lysates, and other necessary reagents were added to a 25–110 Kd Chip, and subsequently loaded onto the Wes detection system. Resulting data was analyzed using Compass software.

RNA isolation—RNA was isolated using TRIZOL reagent or QIAGEN's RNeasy micro Kit and processed according to the manufacturer's protocol.

qPCR Gene Expression Analysis—cDNA was generated using the SuperScript IV VILO cDNA synthesis Kit, and quantitative PCR of desired target genes was performed with the SybrGreen Master Mix reagent. qPCR plates were run and analyzed on an ABI 7500 platform or QuantStudio 6 Flex (Thermo Fisher) qRT-PCR machine. Relative expression and Fold-Difference was determined using the delta-delta-Ct method.

Microarray data acquisition and bioinformatic analysis—RNA was isolated from Fresh and 5-day cultured Satellite Cells and then assayed on an Affymetrix GeneChip Mouse Gene 1.0 ST array according to the manufacturer's protocol. Resulting microarray data was processed and analyzed using the Bioconductor package in the R-statistical programming environment. Specifically, microarray data was normalized using the Robust Multi-Array Average (RMA) method (Bolstad et al., 2003) from the “Oligo” R package, and differentially expressed genes (DEGs) (> 2-fold changed, FDR < 0.02) were calculated with the Limma R package (Ritchie et al., 2015). Annotated Transcription Factors (TFs) from the AnimalTFDB^{2.0} (database) were extracted from the Fresh SC-enriched genes. The bioinformatic pipeline described above was used to re-analyze the microarray data from (Liu et al., 2013) comparing Fresh SCs from injured (BaCl₂) versus uninjured skeletal muscle (Figures S2A and S2B).

RNA-seq data acquisition and bioinformatic analysis—RNA was extracted from 1000 sorted Fresh SCs per replicate per condition (Fos^{GFP+/GFP-}, Fos^{cKO}/Control, Fos^{GFP}/WT Littermate). cDNA libraries were prepared and amplified using Smart-Seq v4 Ultra Low Input RNA Kit for sequencing, and fragmented, adaptor tagged, amplified, and

barcoded using the Nextera XT Kit. Pooled libraries were then quantified using a 2100 BioAnalyzer, and then subjected to massively, paralleled sequencing on Illumina's HiSeq 2500 platform.

FASTQ files were aligned to the mouse reference genome (Ensembl GRCm38.87 assembly) using the STAR (2.5.0c) aligner software with default parameters and exported into BAM format (Dobin et al., 2013). We obtained 18–35 million reads per sample, with greater than 80% mapping efficiency. BAM files of aligned data were converted to SAM format using SAMtools. HTSeq was used to count the number of aligned reads per gene, specifically using the htseq-count function with options -s (no), -m (intersectionnonempty), -t (“Exons”) (Anders et al., 2015). To calculate differential gene expression, gene read count tables generated by HTSeq were used as input for the R package DESeq2 (Love et al., 2014). Differentially expressed genes were defined as those genes displaying > 1.5 (Fos^{GFP+}/GFP^-) or > 2 ($Fos^{cKO}/Control$) Fold-Changed in either direction with an adjusted p value < 0.05 (Benjamin-Hochberg).

For the analysis using RNA-Seq data derived from human Fresh and cultured SCs (Charville et al., 2015), we applied the same bioinformatic pipeline described above, defining Transcription Factors (TFs) enriched in Human Fresh SCs as those increased > 2 -fold (relative to cultured SCs) with an adjusted p value < 0.05 (Figures S2E and S2F). For the analysis using RNA-Seq data derived from mouse, “Alpha7-positive” Fresh and Cultured SCs, a processed matrix containing RPKM values for each gene and each replicate was obtained from a prior study (Ryall et al., 2015; Figures S2C and S2D; Figure 1D). TF mRNAs with at least a 2-fold increase in Fresh relative to Cultured SCs were defined as enriched TFs in Fresh SC.

We identified top ranked Biocarta gene pathways (adjusted p values < 0.05) among enriched gene-sets (as defined by DeSeq2 analysis) using Enrichr (Kuleshov et al., 2016). To identify top ranked Gene Ontology (GO) Terms from the biological process category, enriched gene-sets (as defined by DeSeq2 analysis) were analyzed using the DAVID Bioinformatics resource web interface. GOterms with p values < 0.05 were reported.

We determined whether an overlap between two gene-sets (i.e., enriched genes in Fresh Fos^{GFP+} SCs overlapping with the depleted genes in Fos^{cKO} Fresh SCs) was statistically significant using the Gene Overlap R package, which uses the Fisher's Exact Test for significance. To obtain the universe of expressed transcripts in our RNA-Seq data (using Ensemble GRCm38.87 annotations), we visualized the average \log_2 -transformed, Transcripts Per kilobase Million (TPM) expression values for each transcript (across all samples being compared) as a density function, and then based on the observed distribution, TPM values greater than 0.5 were defined as expressed ($n = 31,253$).

QUANTIFICATION AND STATISTICAL ANALYSIS

Statistical analysis was performed using the Prism GraphPad software and excel. The exact number of cells, the precise number of n (i.e., number of mice used for a particular experiment), and the statistical test used to support the conclusions of a given experiment is reported in the figure legends. P values < 0.05 were defined as statistically significant.

Supplementary Material

Refer to Web version on PubMed Central for supplementary material.

ACKNOWLEDGMENTS

We thank Tommy Vierbuchen, Marty Yang, and Michael E. Greenberg for providing *Fos^{fl/fl}* animals and aliquots of their anti-FOS ChIP-grad antibody as well as for thoughtful discussions throughout the study. We thank Davide Cacchiarelli for technical assistance with generating RNA-seq libraries. Our graphical abstract was created using BioRender. This study was supported by an NIH training grant award (2T32DK007260) (to N.H.), Banting postdoctoral fellowship and funds from the Harvard Program in Therapeutic Science and HMS Laboratory of System Pharmacology (to F.D.P.), the NIH (ES024935 and AG048917) and the Glenn Foundation for Medical Research (to A.J.W.), and by a postdoctoral enrichment award from the Burroughs Wellcome Fund, NIH diversity supplement award (3R01AG048917-02S1), and NIH training grant award (5T32DK007260) (to A.E.A.).

DECLARATION OF INTERESTS

A.J.W. is a scientific advisor for Frequency Therapeutics, and A.J.W. and L.L.R. are co-founders and scientific advisory board members and hold private equity in Elevian, Inc., a company that aims to develop medicines to restore regenerative capacity. Elevian also provides sponsored research to the Wagers lab.

REFERENCES

- Anders S, Pyl PT, and Huber W. (2015). HTSeq—a Python framework to work with high-throughput sequencing data. *Bioinformatics* 31, 166–169. [PubMed: 25260700]
- Barth AL, Gerkin RC, and Dean KL (2004). Alteration of neuronal firing properties after in vivo experience in a FosGFP transgenic mouse. *J. Neurosci* 24, 6466–6475. [PubMed: 15269256]
- Bentzinger CF, Wang YX, von Maltzahn J, Soleimani VD, Yin H, and Rudnicki MA (2013). Fibronectin regulates Wnt7a signaling and satellite cell expansion. *Cell Stem Cell* 12, 75–87. [PubMed: 23290138]
- Bjornson CR, Cheung TH, Liu L, Tripathi PV, Steeper KM, and Rando TA (2012). Notch signaling is necessary to maintain quiescence in adult muscle stem cells. *Stem Cells* 30, 232–242. [PubMed: 22045613]
- Bolstad BM, Irizarry RA, Astrand M, and Speed TP (2003). A comparison of normalization methods for high density oligonucleotide array data based on variance and bias. *Bioinformatics* 19, 185–193. [PubMed: 12538238]
- Brown JR, Nigh E, Lee RJ, Ye H, Thompson MA, Saudou F, Pestell RG, and Greenberg ME (1998). Fos family members induce cell cycle entry by activating cyclin D1. *Mol. Cell. Biol* 18, 5609–5619. [PubMed: 9710644]
- Cerletti M, Jurga S, Witczak CA, Hirshman MF, Shadrach JL, Goodyear LJ, and Wagers AJ (2008). Highly efficient, functional engraftment of skeletal muscle stem cells in dystrophic muscles. *Cell* 134, 37–47. [PubMed: 18614009]
- Chakkalakal JV, Jones KM, Basson MA, and Brack AS (2012). The aged niche disrupts muscle stem cell quiescence. *Nature* 490, 355–360. [PubMed: 23023126]
- Chakkalakal JV, Christensen J, Xiang W, Tierney MT, Boscolo FS, Sacco A, and Brack AS (2014). Early forming label-retaining muscle stem cells require p27kip1 for maintenance of the primitive state. *Development* 141, 1649–1659. [PubMed: 24715455]
- Charville GW, Cheung TH, Yoo B, Santos PJ, Lee GK, Shrager JB, and Rando TA (2015). Ex Vivo Expansion and In Vivo Self-Renewal of Human Muscle Stem Cells. *Stem Cell Reports* 5, 621–632. [PubMed: 26344908]
- Cohen MS, and Chang P. (2018). Insights into the biogenesis, function, and regulation of ADP-ribosylation. *Nat. Chem. Biol* 14, 236–243. [PubMed: 29443986]
- Collins CA, Olsen I, Zammit PS, Heslop L, Petrie A, Partridge TA, and Morgan JE (2005). Stem cell function, self-renewal, and behavioral heterogeneity of cells from the adult muscle satellite cell niche. *Cell* 122, 289–301. [PubMed: 16051152]

- Dobin A, Davis CA, Schlesinger F, Drenkow J, Zaleski C, Jha S, Batut P, Chaisson M, and Gingeras TR (2013). STAR: ultrafast universal RNA-seq aligner. *Bioinformatics* 29, 15–21. [PubMed: 23104886]
- Dull T, Zufferey R, Kelly M, Mandel RJ, Nguyen M, Trono D, and Naldini L. (1998). A third-generation lentivirus vector with a conditional packaging system. *J. Virol* 72, 8463–8471. [PubMed: 9765382]
- Dumont NA, Wang YX, von Maltzahn J, Pasut A, Bentzinger CF, Brun CE, and Rudnicki MA (2015). Dystrophin expression in muscle stem cells regulates their polarity and asymmetric division. *Nat. Med* 21, 1455–1463. [PubMed: 26569381]
- Fleischmann A, Hvalby O, Jensen V, Strelakova T, Zacher C, Layer LE, Kvello A, Reschke M, Spanagel R, Sprengel R, et al. (2003). Impaired long-term memory and NR2A-type NMDA receptor-dependent synaptic plasticity in mice lacking c-Fos in the CNS. *J. Neurosci* 23, 9116–9122. [PubMed: 14534245]
- Friedrich M, Böhlig L, Kirschner RD, Engeland K, and Hauschildt S. (2008). Identification of two regulatory binding sites which confer myotube specific expression of the mono-ADP-ribosyltransferase ART1 gene. *BMC Mol. Biol* 9, 91. [PubMed: 18939989]
- Greenberg ME, and Ziff EB (1984). Stimulation of 3T3 cells induces transcription of the c-fos proto-oncogene. *Nature* 311, 433–438. [PubMed: 6090941]
- Igarashi M, Miura M, Williams E, Jaksch F, Kadowaki T, Yamauchi T, and Guarente L. (2019). NAD⁺ supplementation rejuvenates aged gut adult stem cells. *Aging Cell* 18, e12935.
- Jones NC, Tyner KJ, Nibarger L, Stanley HM, Cornelison DD, Fedorov YV, and Olwin BB (2005). The p38alpha/beta MAPK functions as a molecular switch to activate the quiescent satellite cell. *J. Cell Biol* 169, 105–116. [PubMed: 15824134]
- Kimmel JC, Hwang AB, Scaramozza A, Marshall WF, and Brack AS (2020). Aging induces aberrant state transition kinetics in murine muscle stem cells. *Development* 147, dev183855.
- Kuang S, Kuroda K, Le Grand F, and Rudnicki MA (2007). Asymmetric self-renewal and commitment of satellite stem cells in muscle. *Cell* 129, 999–1010. [PubMed: 17540178]
- Kuleshov MV, Jones MR, Rouillard AD, Fernandez NF, Duan Q, Wang Z, Koplev S, Jenkins SL, Jagodnik KM, Lachmann A, et al. (2016). Enrichr: a comprehensive gene set enrichment analysis web server 2016 update. *Nucleic Acids Res.* 44 (W1), W90–7. [PubMed: 27141961]
- Lepper C, Partridge TA, and Fan CM (2011). An absolute requirement for Pax7-positive satellite cells in acute injury-induced skeletal muscle regeneration. *Development* 138, 3639–3646. [PubMed: 21828092]
- Leutert M, Menzel S, Braren R, Rissiek B, Hopp AK, Nowak K, Bisceglie L, Gehrig P, Li H, Zolkiewska A, et al. (2018). Proteomic Characterization of the Heart and Skeletal Muscle Reveals Widespread Arginine ADP-Ribosylation by the ARTC1 Ectoenzyme. *Cell Rep.* 24, 1916–1929.e5. [PubMed: 30110646]
- Liu L, Cheung TH, Charville GW, Hurgo BM, Leavitt T, Shih J, Brunet A, and Rando TA (2013). Chromatin modifications as determinants of muscle stem cell quiescence and chronological aging. *Cell Rep.* 4, 189–204. [PubMed: 23810552]
- Loesberg C, van Rooij H, and Smets LA (1990). Meta-iodobenzyl-guanidine (MIBG), a novel high-affinity substrate for cholera toxin that interferes with cellular mono(ADP-ribosylation). *Biochim. Biophys. Acta* 1037, 92–99. [PubMed: 2104758]
- Love MI, Huber W, and Anders S. (2014). Moderated estimation of fold change and dispersion for RNA-seq data with DESeq2. *Genome Biol.* 15, 550. [PubMed: 25516281]
- Machado L, Esteves de Lima J, Fabre O, Proux C, Legendre R, Szegedi A, Varet H, Ingerslev LR, Barrès R, Relaix F, and Mourikis P. (2017). In Situ Fixation Redefines Quiescence and Early Activation of Skeletal Muscle Stem Cells. *Cell Rep.* 21, 1982–1993. [PubMed: 29141227]
- Madisen L, Zwingman TA, Sunkin SM, Oh SW, Zariwala HA, Gu H, Ng LL, Palmiter RD, Hawrylycz MJ, Jones AR, et al. (2010). A robust and high-throughput Cre reporting and characterization system for the whole mouse brain. *Nat. Neurosci* 13, 133–140. [PubMed: 20023653]
- Maesner CC, Almada AE, and Wagers AJ (2016). Established cell surface markers efficiently isolate highly overlapping populations of skeletal muscle satellite cells by fluorescence-activated cell sorting. *Skelet. Muscle* 6, 35. [PubMed: 27826411]

- Mauro A. (1961). Satellite cell of skeletal muscle fibers. *J. Biophys. Biochem. Cytol* 9, 493–495. [PubMed: 13768451]
- Montarras D, Morgan J, Collins C, Relaix F, Zaffran S, Cumano A, Partridge T, and Buckingham M. (2005). Direct isolation of satellite cells for skeletal muscle regeneration. *Science* 309, 2064–2067. [PubMed: 16141372]
- Pasut A, Jones AE, and Rudnicki MA (2013). Isolation and culture of individual myofibers and their satellite cells from adult skeletal muscle. *J. Vis. Exp* (73), e50074.
- Ritchie ME, Phipson B, Wu D, Hu Y, Law CW, Shi W, and Smyth GK (2015). limma powers differential expression analyses for RNA-sequencing and microarray studies. *Nucleic Acids Res.* 43, e47. [PubMed: 25605792]
- Rocheteau P, Gayraud-Morel B, Siegl-Cachedenier I, Blasco MA, and Tajbakhsh S. (2012). A subpopulation of adult skeletal muscle stem cells retains all template DNA strands after cell division. *Cell* 148, 112–125. [PubMed: 22265406]
- Rodgers JT, King KY, Brett JO, Cromie MJ, Charville GW, Maguire KK, Brunson C, Mastey N, Liu L, Tsai CR, et al. (2014). mTORC1 controls the adaptive transition of quiescent stem cells from G0 to G(Alert). *Nature* 510, 393–396. [PubMed: 24870234]
- Ryall JG, Dell’Orso S, Derfoul A, Juan A, Zare H, Feng X, Clermont D, Koulonis M, Gutierrez-Cruz G, Fulco M, and Sartorelli V. (2015). The NAD(+)-dependent SIRT1 deacetylase translates a metabolic switch into regulatory epigenetics in skeletal muscle stem cells. *Cell Stem Cell* 16, 171–183. [PubMed: 25600643]
- Ryu D, Zhang H, Ropelle ER, Sorrentino V, Mázala DA, Mouchiroud L, Marshall PL, Campbell MD, Ali AS, Knowels GM, et al. (2016). NAD+ repletion improves muscle function in muscular dystrophy and counters global PARylation. *Sci. Transl. Med* 8, 361ra139.
- Sacco A, Doyonnas R, Kraft P, Vitorovic S, and Blau HM (2008). Selfrenewal and expansion of single transplanted muscle stem cells. *Nature* 456, 502–506. [PubMed: 18806774]
- Sambasivan R, Yao R, Kissenpennig A, Van Wittenberghe L, Paldi A, Gayraud-Morel B, Guenou H, Malissen B, Tajbakhsh S, and Galy A. (2011). Pax7-expressing satellite cells are indispensable for adult skeletal muscle regeneration. *Development* 138, 3647–3656. [PubMed: 21828093]
- Seale P, Sabourin LA, Girgis-Gabardo A, Mansouri A, Gruss P, and Rudnicki MA (2000). Pax7 is required for the specification of myogenic satellite cells. *Cell* 102, 777–786. [PubMed: 11030621]
- Shea KL, Xiang W, LaPorta VS, Licht JD, Keller C, Basson MA, and Brack AS (2010). Sprouty1 regulates reversible quiescence of a selfrenewing adult muscle stem cell pool during regeneration. *Cell Stem Cell* 6, 117–129. [PubMed: 20144785]
- Shelton M, Ritso M, Liu J, O’Neil D, Kocharyan A, Rudnicki MA, Stanford WL, Skerjanc IS, and Blais A. (2019). Gene expression profiling of skeletal myogenesis in human embryonic stem cells reveals a potential cascade of transcription factors regulating stages of myogenesis, including quiescent/activated satellite cell-like gene expression. *PLoS ONE* 14, e0222946.
- Sherwood RI, Christensen JL, Conboy IM, Conboy MJ, Rando TA, Weissman IL, and Wagers AJ (2004). Isolation of adult mouse myogenic progenitors: functional heterogeneity of cells within and engrafting skeletal muscle. *Cell* 119, 543–554. [PubMed: 15537543]
- Shin KJ, Wall EA, Zavzavadjian JR, Santat LA, Liu J, Hwang JI, Rebres R, Roach T, Seaman W, Simon MI, and Fraser ID (2006). A single lentiviral vector platform for microRNA-based conditional RNA interference and coordinated transgene expression. *Proc. Natl. Acad. Sci. USA* 103, 13759–13764.
- van den Brink SC, Sage F, Vértesy Á., Spanjaard B, Peterson-Maduro J, Baron CS, Robin C, and van Oudenaarden A. (2017). Single-cell sequencing reveals dissociation-induced gene expression in tissue subpopulations. *Nat. Methods* 14, 935–936. [PubMed: 28960196]
- van Velthoven CTJ, de Morree A, Egner IM, Brett JO, and Rando TA (2017). Transcriptional Profiling of Quiescent Muscle Stem Cells In Vivo. *Cell Rep.* 21, 1994–2004. [PubMed: 29141228]
- Vannini N, Campos V, Girotra M, Trachsel V, Rojas-Sutterlin S, Tratwal J, Ragusa S, Stefanidis E, Ryu D, Rainer PY, et al. (2019). The NADB-ooster Nicotinamide Riboside Potently Stimulates Hematopoiesis through Increased Mitochondrial Clearance. *Cell Stem Cell* 24, 405–418.e7. [PubMed: 30849366]

- Wright DE, Wagers AJ, Gulati AP, Johnson FL, and Weissman IL (2001). Physiological migration of hematopoietic stem and progenitor cells. *Science* 294, 1933–1936. [PubMed: 11729320]
- Xu JX, Xiong W, Zeng Z, Tang Y, Wang YL, Xiao M, Li M, Li QS, Song GL, and Kuang J. (2017). Effect of ART1 on the proliferation and migration of mouse colon carcinoma CT26 cells in vivo. *Mol. Med. Rep* 15, 1222–1228. [PubMed: 28138708]
- Zammit PS, Golding JP, Nagata Y, Hudon V, Partridge TA, and Beauchamp JR (2004). Muscle satellite cells adopt divergent fates: a mechanism for self-renewal? *J. Cell Biol* 166, 347–357. [PubMed: 15277541]
- Zhang H, Ryu D, Wu Y, Gariani K, Wang X, Luan P, D’Amico D, Ropelle ER, Lutolf MP, Aebbersold R, et al. (2016). NAD⁺ repletion improves mitochondrial and stem cell function and enhances life span in mice. *Science* 352, 1436–1443. [PubMed: 27127236]

Highlights

- Injury-exposed satellite cells (SCs) rapidly and transiently induce FOS
- FOS-expressing SCs activate faster and display superior regenerative activity
- *Fos*-null SCs activate more slowly and have diminished regenerative activity
- The FOS target *Art1* is required for efficient SC activation and muscle repair

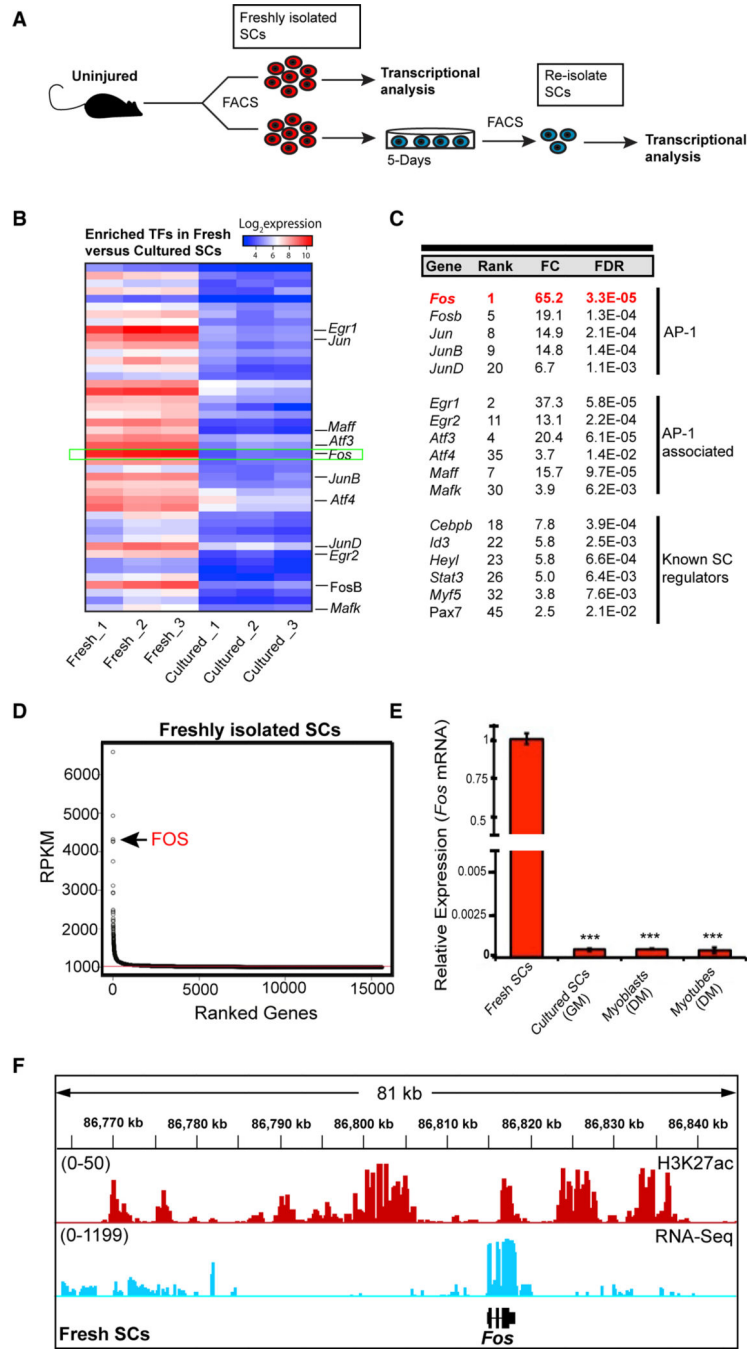


Figure 1. Abundant *Fos* mRNA is a feature of SCs freshly isolated from uninjured skeletal muscle

(A) Experimental strategy for transcriptional profiling of fresh SCs from uninjured skeletal muscle and 5-day cultured SCs (cells from 3 mice).

(B) Clustered heatmap (dendrograms not shown) showing 45 transcription factors (TFs) enriched (>2-fold change, FDR < 0.02) in fresh relative to cultured SCs. AP-1 and AP-1-associated TFs are highlighted.

(C) The most enriched and notable TFs in fresh SCs along with their rank (i.e., enrichment in fresh SCs), fold change (FC), and false discovery rate (FDR).

(D) All mRNAs detected in fresh SCs ranked by reads per kilobase of transcript per million mapped reads (RPKM) expression. RPKM values for duplicate RNA-seq datasets from fresh SCs were averaged for each gene as in Ryall et al. (2015).

(E) qPCR showing mean (\pm SD) relative *Fos* mRNA expression (normalized to glyceraldehyde 3-phosphate dehydrogenase [GAPDH]) in fresh SCs from uninjured skeletal muscle, 5-day cultured SCs in GM, differentiating myoblasts in differentiation medium (DM) for 24 h, and terminal myotubes in DM for 72 h (cells from 3 mice). One-way ANOVA with Tukey post hoc test, *** $p < 0.001$ comparing fresh SCs with all other conditions.

(F) Genome view around the *Fos* locus, displaying RNA-seq read count density and H3K27ac (chromatin immunoprecipitation sequencing [ChIP-seq]) read coverage. See also Figures S1 and S2.

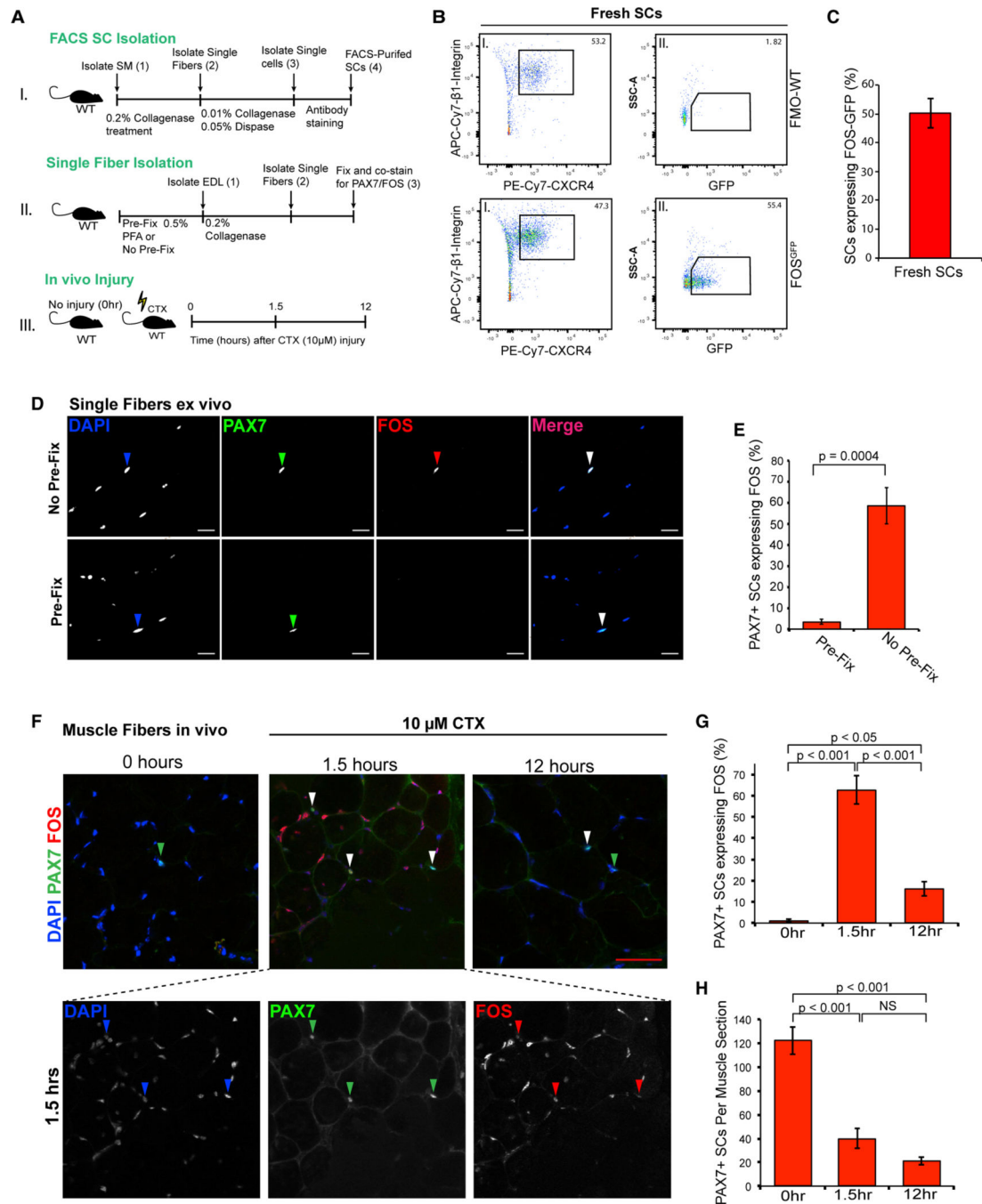


Figure 2. FOS is transiently and heterogeneously induced in SCs within hours after muscle trauma

(A) Workflow for isolating fresh SCs (I) and single fibers (II) from skeletal muscle and time points included in the *in vivo* injury time course (III).

(B) Dot plots showing analysis for (II) GFP expression in CD45⁻/CD11b⁻/Ter119⁻/CD31⁻/Sca1⁻/ β 1-Integrin⁺/CXCR4⁺ fresh SCs (I) from uninjured muscles of wild-type (FMO-WT, top) or Fos^{GFP} (bottom) mice. SSC-A, side scatter area. Data were pre-gated on physical and live cell parameters (see STAR methods for details).

(C) Mean (\pm SD) percentage of fresh Fos^{GFP} SCs expressing GFP (compiled analysis from 15 mice).

(D) Pre-fixed (bottom) or non-pre-fixed (standard isolation, top) single fibers co-stained for PAX7 (green), FOS (red), and DAPI (blue).

(E) Quantification (mean \pm SD) of the percentage of PAX7+ SCs expressing FOS in freshly isolated single fibers stained as in (D). Data represent enumeration of more than 100 SCs across a minimum of 30 fibers per biological replicate for each condition (n = 3 mice per condition).

(F) Fresh-frozen muscle sections co-stained for PAX7 (green), FOS (red), and DAPI (blue) 0, 1.5, and 12 h after cardiotoxin (CTX; 10 μ M) injury. All channels are shown separately for the 1.5 h post-injury field (bottom row) and merged for 0, 1.5, and 12 h (top row).

(G and H) Quantification of immunofluorescence (IF) data shown in (F), including (G) mean (\pm SD) percentage of PAX7+ SCs expressing FOS protein and (H) mean (\pm SD) number of PAX7+ SCs quantified per TA/*extensor digitorum longus* (EDL) section per condition (n = 3 mice per time point).

Student's two-tailed unpaired t test (E) and one-way ANOVA with Tukey post hoc test (G and H). The scale bars represent 50 μ m (D) and 100 μ m (F). See also Figure S3.

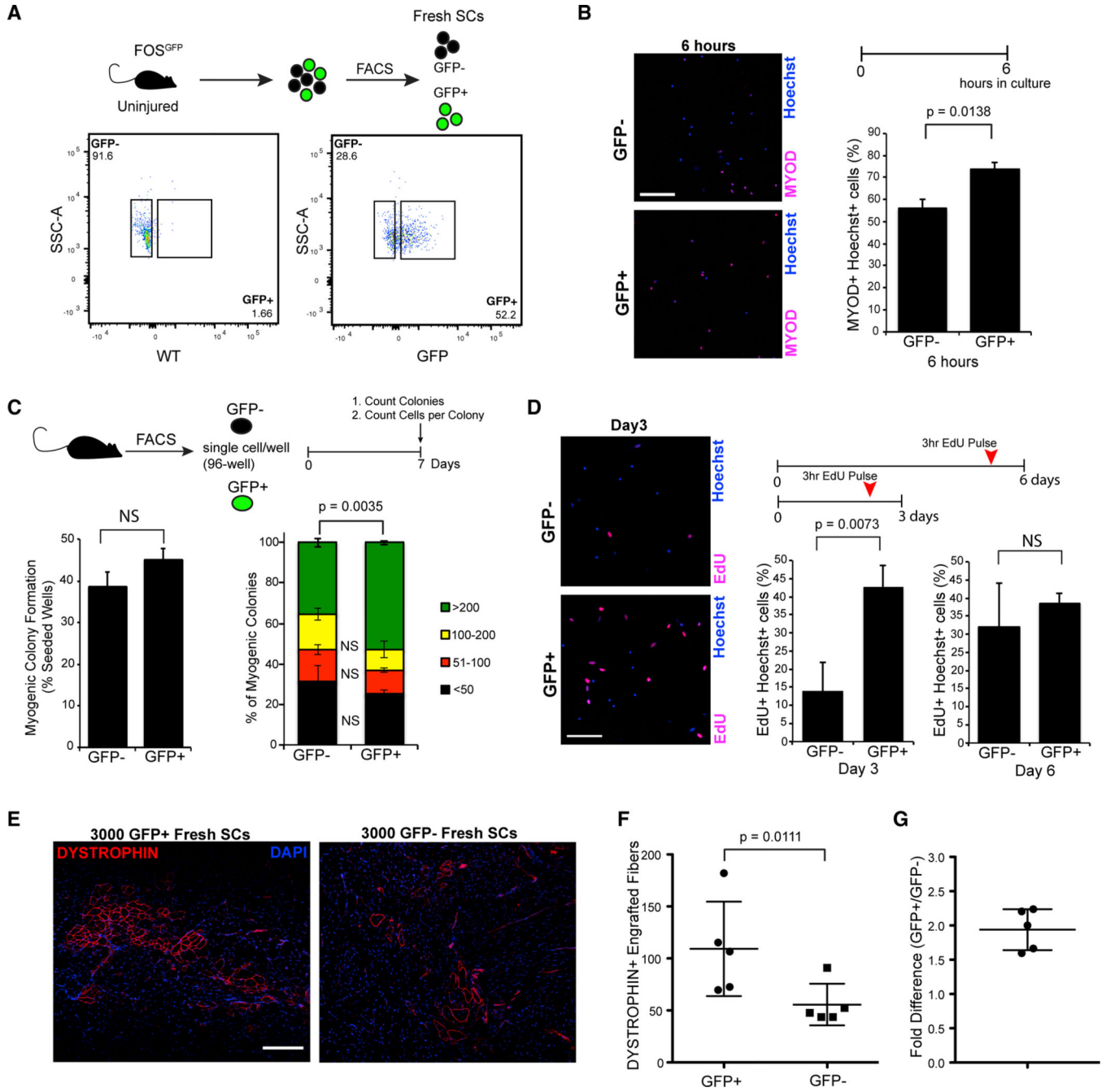


Figure 3. FOS^{GFP} marks a subset of SCs with enhanced regenerative activity
 (A) Gating strategy for sorting CD45⁻/CD11b⁻/Ter119⁻/CD31⁻/Sca1⁻/β1-integrin⁺/CXCR4⁺ fresh FOS^{GFP-} and FOS^{GFP+} SCs based on a fluorescence minus one (FMO) control (SCs from WT mice). Data were pre-gated on physical and live cell parameters (see STAR methods for details).
 (B) 2,000 FOS^{GFP-} or 2,000 FOS^{GFP+} SCs were cultured in growth medium (GM) for 6 h prior to IF for MYOD (magenta). Hoechst is shown in blue. Also shown is the mean (±SD) percentage of MYOD+ cells after 6 h in culture (analysis from 3 mice).

(C) Mean (\pm SD) percentage of single GFP⁺ or GFP⁻ cells that gave rise to viable myogenic colonies (left) and to colonies containing more than 200, 100–200, 50–100, and fewer than 50 cells per colony (right). A total of 82 and 86 colonies for Fos^{GFP-} and Fos^{GFP+} cells were quantified, respectively (cells from 2 mice).

(D) 2,000 Fos^{GFP+} and 2,000 Fos^{GFP-} fresh SCs cultured in GM for 3 days and pulsed with EdU 3 h before harvest, showing EdU⁺ (magenta) and Hoechst⁺ (blue) nuclei. Shown is the mean (\pm SD) percentage of EdU⁺ nuclei among total Hoechst⁺ nuclei after 3 or 6 days in culture (n = 3 mice each time point).

(E) Regenerating TA muscle transplanted with 3,000 fresh Fos^{GFP+} or 3000 Fos^{GFP-} SCs 3 weeks prior.

(F and G) Total number of engrafted DYSTROPHIN⁺ (red) muscle fibers (F) and fold difference in DYSTROPHIN⁺ muscle fiber engraftment (G) upon transplantation with Fos^{GFP+} or Fos^{GFP-} cells from the same donor (n = 5 donor and recipient mice). Dots represent data for individual recipient animals overlaid with mean \pm SD.

Student's two-tailed unpaired (B–D) and paired (F) t test. Scale bars, 100 mm (B and D) and 200 μ m (E). See also Figure S4.

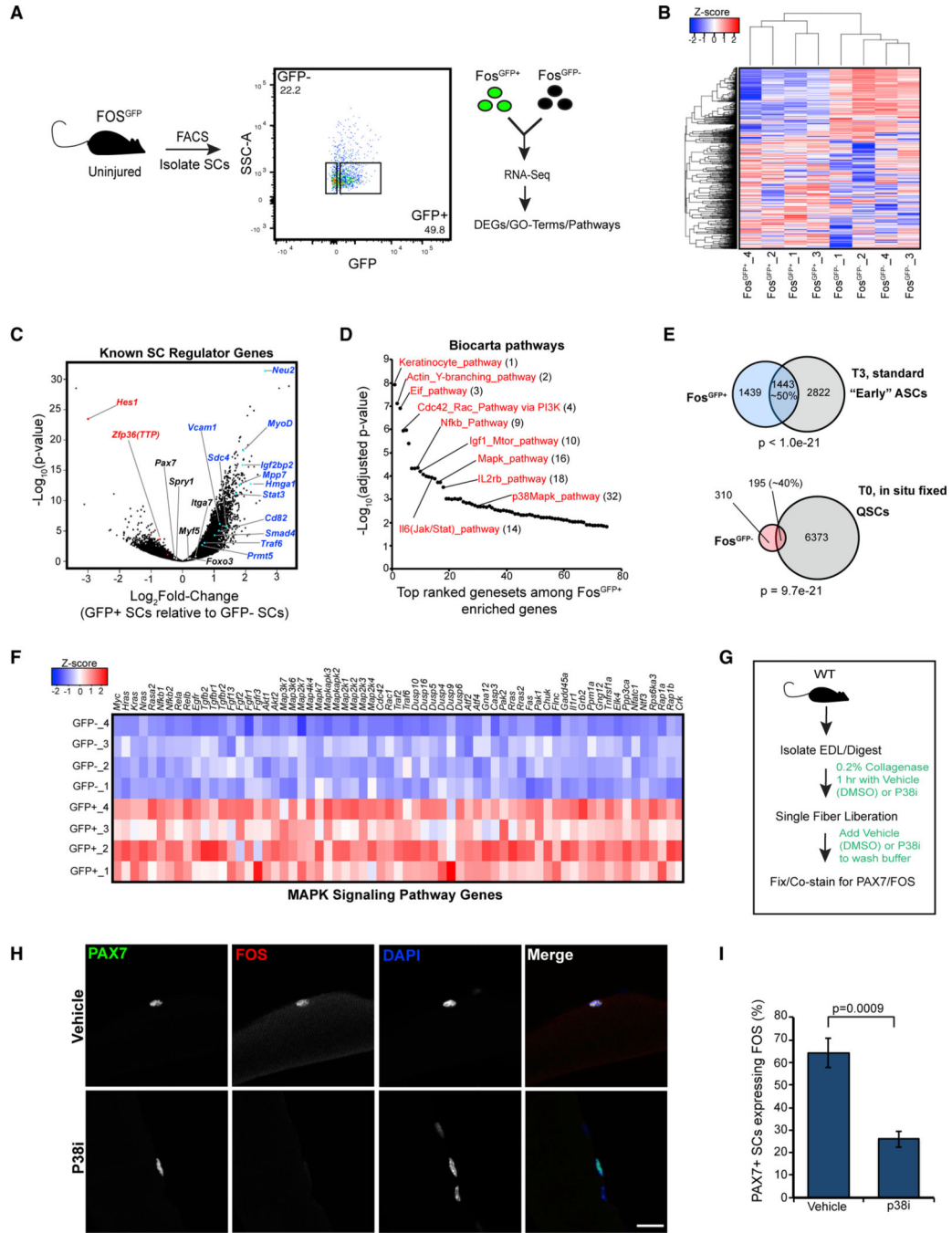


Figure 4. Fresh Fos^{GFP+} SCs express a pro-regenerative transcriptional gene signature
 (A) Schematic showing the experimental design and FACS gating strategy for isolation of 1,000 Fresh Fos^{GFP+} and 1,000 Fos^{GFP-} SCs directly sorted for RNA-seq analysis (SCs isolated from 4 mice).
 (B) Hierarchically clustered heatmap showing all 3,387 differentially expressed genes (DEGs; >1.5 FC, FDR < 0.05) in Fos^{GFP+} versus Fos^{GFP-} SCs.
 (C) Volcano plot highlighting known SC regulator genes enriched (blue) or depleted (red) in fresh Fos^{GFP+} SCs. Notable mRNAs not significantly changed are indicated in black.

- (D) Top ranked Biocarta pathways associated with enriched genes in Fos^{GFP+} fresh SCs.
- (E) Venn diagrams showing overlap in genes enriched in Fos^{GFP+} or Fos^{GFP-} SCs and in T3 (standard isolation, top) or T0 (*in-situ-fixed*, quiescent SCs, bottom) SCs, respectively (Machado et al., 2017). The p values were determined by Fisher's exact test of significance.
- (F) Heatmap of MAPK targets expressed in Fos^{GFP+} SCs relative to Fos^{GFP-} SCs.
- (G) Strategy for testing whether p38 MAPK induces FOS in freshly isolated single fibers.
- (H) Single fibers co-stained for PAX7 and FOS after isolation in the presence of vehicle or the p38 MAPK inhibitor SB202190 (SB). Scale bar, 50 μ m.
- (I) Mean (\pm SD) percentage of PAX7+ SCs expressing FOS protein after isolation under the indicated condition. Data represent enumeration of more than 100 SCs across a minimum of 30 fibers per biological replicate for each condition (n = 3 mice per condition). The Z score equals the number of SDs from the mean expression of all genes (C and F). Fisher's exact test (E) and Student's two-tailed unpaired t test (I). See also Figure S5.

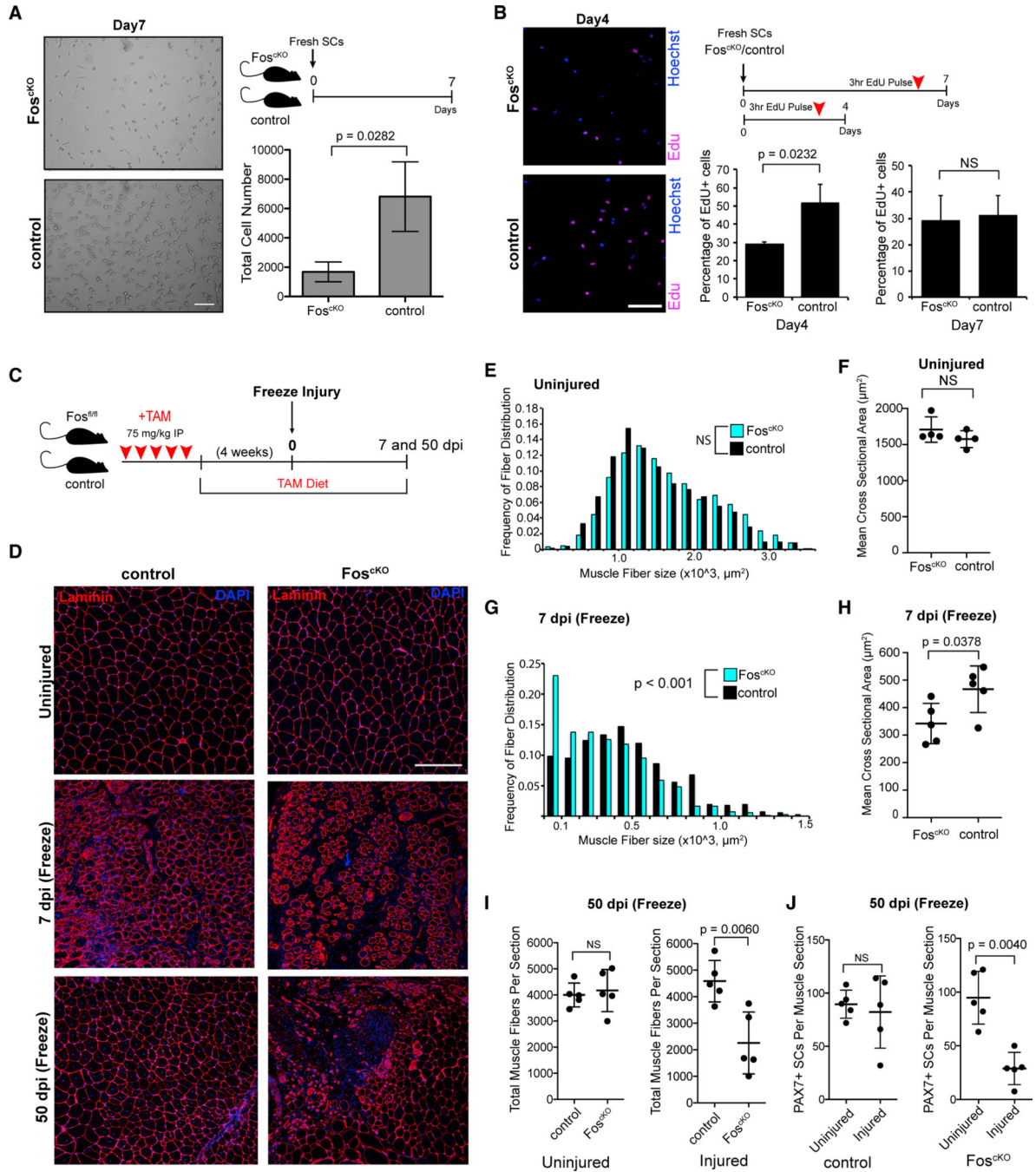


Figure 5. *Fos^{CKO}* SCs display diminished regenerative activity

(A) 1,500 *Fos^{CKO}* or 1,500 fresh control SCs were cultured for 7 days in GM. Shown is quantification of the mean (\pm SD) number of Hoechst+ cells per well (*n* = 3 mice per genotype).

(B) 2,000 fresh *Fos^{CKO}* or 2,000 control SCs cultured in GM for 4 or 7 days and pulsed with EdU 3 hr before harvest, displaying EdU-positive (magenta) and Hoechst-positive (blue) nuclei and mean (\pm SD) percentage of EdU+ nuclei among total Hoechst+ cells after 4 (*n* = 2–4 mice per genotype) or 7 days (*n* = 3 mice per genotype) in culture.

(C) Schematic showing the tamoxifen (TAM) treatment regimen before and after a freeze muscle injury (cryoinjury) in the TA muscle.

(D) Representative Laminin-stained Fos^{cKO} and control muscle sections (20×) from uninjured mice (top) and from mice 7 (center) and 50 (bottom) days after freeze injury.

(E and F) Distribution (E) and mean (\pm SD) cross-sectional area (CSA; F) of fiber sizes from uninjured Fos^{cKO} or control animals (n = 4 mice per genotype).

(G and H) Distribution (G) and mean (\pm SD) CSA (H) of regenerating (centrally nucleated) muscle fibers 7 days after freeze injury (n = 5 mice per genotype).

(I) Quantification of the total number of muscle fibers per TA/EDL section in control and Fos^{cKO} mice before (left) and 50 days after freeze injury (right) (n = 5 mice per genotype per condition).

(J) Total number of Pax7+ SCs in uninjured and injured (50 dpi, freeze) TA/EDL muscle sections of control (left) and Fos^{cKO} mice (right) (n = 5 mice per genotype per condition). Dots represent data for individual control or Fos^{cKO} animals overlaid with mean \pm SD. Student's two-tailed unpaired (A, B, F, H, and I) and paired (J) t test and Mann-Whitney *U* test (E and G). Scale bars, 100 μ m (A, B, and D). See also Figure S6.

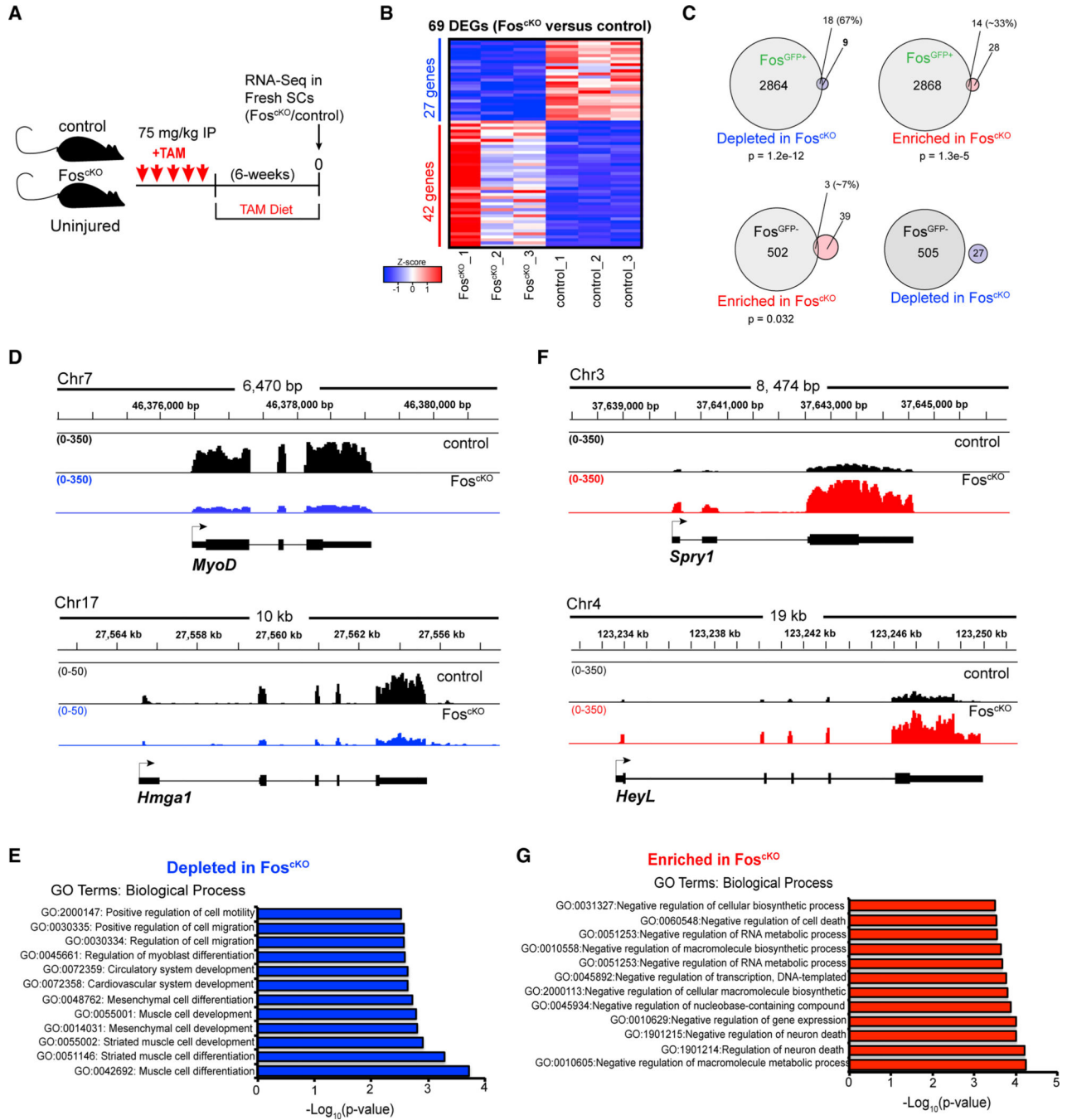


Figure 6. Fos^{CKO} SCs fail to induce the early-activated pro-regenerative transcriptional program

(A) 1,000 Fos^{CKO} and 1,000 fresh control SCs were directly sorted from uninjured muscle tissue for RNA-seq analysis.

(B) Clustered heatmap (dendrogram not shown) displaying 69 DEGs (>2-fold with FDR < 0.05) between Fos^{CKO} and control SCs. The Z score equals the number of SDs from the mean expression of all genes.

(C) Venn diagrams indicating overlap of all comparisons between Fos^{GFP+} and Fos^{GFP-} enriched genes, with 27 genes depleted in Fos^{cKO} SCs and 42 genes enriched in Fos^{cKO} SCs. The p values represent Fisher's exact test of significance.

(D and F) Genome view showing RNA-seq read count density around (D) *MyoD* and *Hmga1* and (F) *Sprouty1* (*Spry1*) and *HeyL* loci.

(E and G) The top 12 enriched Gene Ontology (GO) terms among genes depleted in Fos^{cKO} cells (E) and genes enriched in Fos^{cKO} cells (G) relative to control cells.

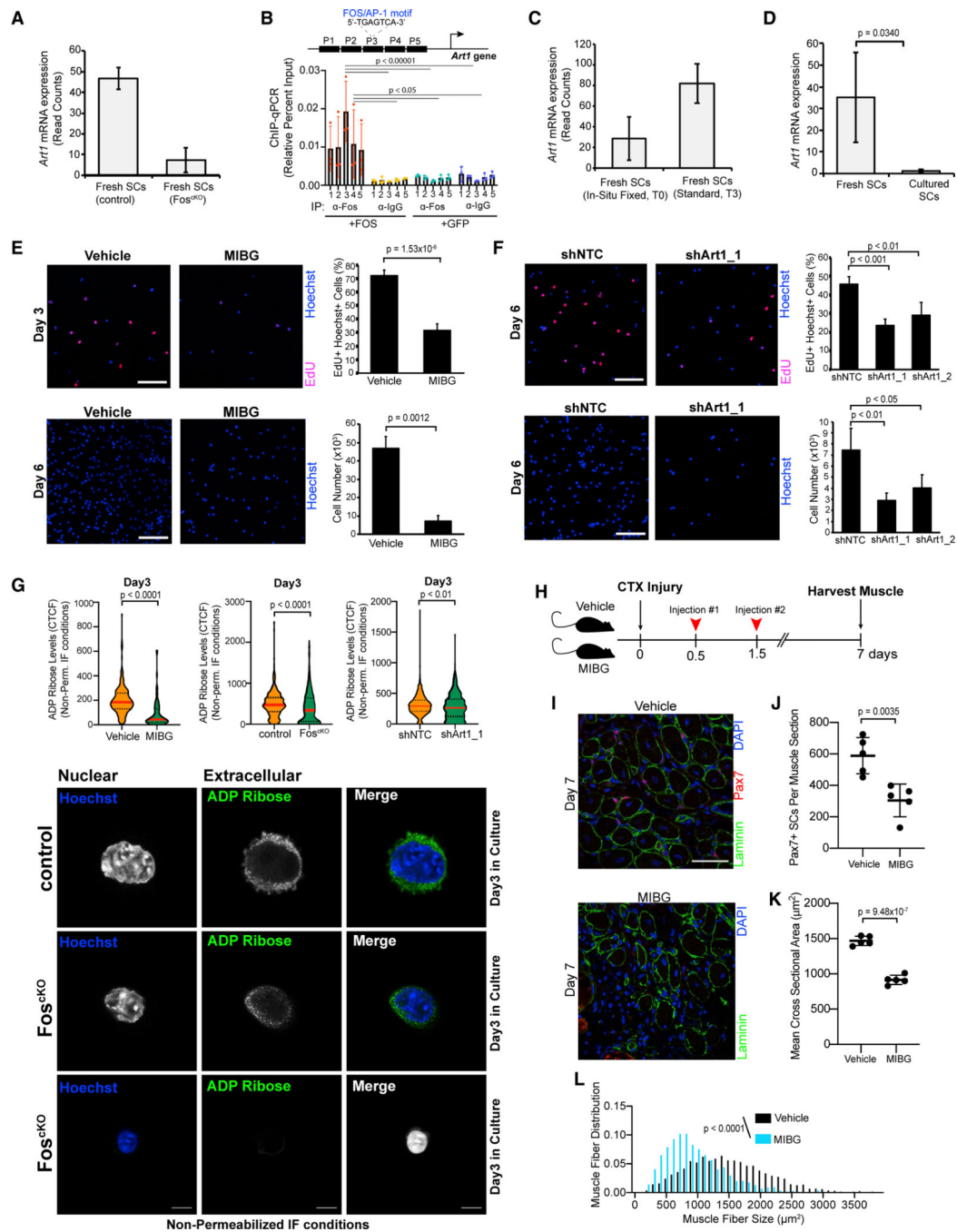


Figure 7. *Art1* is a direct FOS target whose pharmacological and genetic disruption impairs SC function

(A) RNA-seq (normalized read counts) showing mean (\pm SD) *Art1* mRNA expression in fresh *Fos*^{ckO} and control SCs.

(B) ChIP-qPCR assays using a FOS or immunoglobulin G (IgG)-only antibody to immunoprecipitate chromatin isolated from cultured SCs ectopically expressing FOS(+FOS) or GFP (+GFP) (n = 3 independent ChIP experiments using SCs from 3 mice). 5 different probes targeted the *Art1* promoter near the FOS/AP-1 DNA motif.

(C) RNA-Seq (normalized read counts) showing mean (\pm SD) *Art1* mRNA expression in fresh SCs isolated from *in-situ*-fixed (T0) or non-pre-fixed (standard, T3) skeletal muscle (Machado et al., 2017).

(D) qPCR showing mean (\pm SD) *Art1* mRNA expression (normalized to GAPDH) in fresh relative to 7-day-cultured SCs.

(E) 3,000 fresh SCs were cultured for 3 days with vehicle or MIBG (50 μ M). Shown are images and quantification of the mean (\pm SD) percentage of EdU+ nuclei among Hoechst+ SCs (top). 3,000 fresh SCs were cultured for 6 days with vehicle or MIBG (50 μ M). Shown are images and quantification of the total number (mean \pm SD) of Hoechst+ nuclei (bottom) (n = 4 mice each condition).

(F) 3,000 fresh SCs were infected with lentivirus on the day of isolation with a non-targeting control (NTC) shRNA or one of two distinct shRNAs targeting *Art1* mRNA and cultured for 6 days. Shown are images and quantification of the mean percentage (\pm SD) of EdU+ nuclei among Hoechst+ nuclei (top) or the total number (mean \pm SD) of Hoechst+ nuclei (bottom) (n = 4 mice per condition).

(G) Distribution of ADP ribosylation levels (corrected total cell fluorescent signal [CTCF]) on individual vehicle/MIBG-treated (left), control/*Fos*^{CKO} (center), and shNTC/sh*Art1*-expressing (right) SCs cultured for 3 days. IF was performed under non-permeabilization conditions to ensure extracellular signal. n = 250 cells (vehicle)/80 cells (MIBG) from 3 mice, n = 588 cells (control)/395 cells (*Fos*^{CKO}) from 4 mice, and n = 1,300 cells (shNTC)/695 cells (*shArt1*) from 4 mice. Red lines represent the median value, and lower and upper black lines represent the first and third quartiles of the data. *shArt1*-expressing SCs have reduced cell-surface ADP ribosylation in a small subset of the population, specifically in the first quartile (highlighted in Figure S7F). Shown are three representative images of cell surface ADP ribosylation (green) on Hoechst+ (blue) control and *Fos*^{CKO} fresh SCs after 3 days in culture.

(H) Experimental design. We performed two consecutive injections for 2 days (1 injection per day) of MIBG (50 μ M) or vehicle into the TA muscle following a CTX injury and then harvested regenerating muscle 7 dpi.

(I) Representative images showing PAX7+ SCs associated with regenerating (centrally nucleated) fibers 7 days after CTX injury. Pax7 (red), nuclei (DAPI), and Laminin (Green) are shown.

(J) Quantification of the total number of PAX7+ SCs per TA/EDL muscle section in vehicle- and MIBG-treated mice (n = 5 mice per treatment).

(K and L) Enumeration of the mean CSA (K) and distribution (L) of regenerating (centrally nucleated) muscle fibers in vehicle- and MIBG-treated mice at 7 dpi (n = 5 mice per condition).

Two-way ANOVA with post hoc Holm-Sidak test (B), one-way ANOVA with Tukey post hoc test (F), Student's two-tailed unpaired t test (D, E, J, and K), and Mann-Whitney *U* test (G and L). Scale bars represent 100 μ m (E and F), 10 mm (G), and 50 μ m (I). See also Figure S7.

KEY RESOURCES TABLE

REAGENT or RESOURCE	SOURCE	IDENTIFIER
Antibodies		
APC anti-mouse Ly-6A/E (Sca-1, Clone E3-161.7)	BioLegend	Cat# 122512; RRID: AB_756197
APC anti-mouse CD31 (Clone 390)	BioLegend	Cat# 102510; RRID: AB_312917
APC anti-mouse CD45 (Clone 30-F11)	BioLegend	Cat# 103112; RRID: AB_312977
APC anti-mouse CD11b (Mac-1) (Clone M1/70)	BioLegend	Cat# 101212; RRID: AB_312795
APC-Cy7 anti-mouse CD29 (Clone HM β 1-1)	BioLegend	Cat# 1022261 RRID: AB_2128076
Biotin anti-mouse CD184 (CXCR4) (Clone 2B11)	BioLegend	Cat# 146516; RRID: AB_2650787
Streptavidin-PeCy7	BioLegend	Cat# 405206; RRID: AB_2737413
Mouse anti-mouse PAX7	DSHB	RRID: AB_528428
Rabbit anti-mouse FOS	Santa Cruz	Cat# sc-7202; RRID:AB_2106765
Rabbit anti-mouse FOS	Abcam	Cat# ab190289; RRID:AB_2737414
Rabbit anti-mouse FOS (For ChIP)	Gift from M. Greenberg Lab, Harvard Medical School	N/A
Rabbit mAP anti-IgG XP, Isotype Control (For ChIP)	Cell Signaling Technology	Cat# 3900S; RRID: AB_1550038
anti-mouse Dystrophin	Abcam	Cat# ab15277; RRID: AB_301813
anti-mouse MyoD1	DAKO	Cat# M3512; RRID: AB_2148874
anti-Rabbit-IgG-AF555	Thermo Fisher	Cat# A-21428; RRID: AB_2535849
Anti-Rabbit-IgG-AF488	Thermo Fisher	Cat# A-11008; RRID: AB_143165
Anti-Mouse-IgG1-AF488	Thermo Fisher	Cat# A-21121; RRID: AB_2535764
Anti-Mouse-IgG-AF647	Thermo Fisher	Cat# A-21235; RRID: AB_2535804
Anti-GAPDH	Santa Cruz	Cat# sc-32233; RRID: AB_627679
Anti-GFP	Abcam	Cat# ab5450; RRID: AB_304897
Anti-ADP-Ribose	Cell Signaling	Cat# 83732; RRID: AB_2749858
Chemicals, peptides, and recombinant proteins		
Collagenase type II	Thermo Fisher	Cat# 17101015
Dispase II	Thermo Fisher	Cat# 17105041
Collagen	MilliporeSigma	Cat# C7661
Laminin	Invitrogen	Cat# 23017-015
Donor Horse Serum	Atlanta Biologicals	Cat# 512150
GlutaMAX	GIBCO	Cat# 35050-061
Penn/Strep	GIBCO	Cat# 15070-063
F10	GIBCO	Cat# 11550043
DMEM	GIBCO	Cat# 11965-092
Human recombinant, bFGF	MilliporeSigma	Cat# F0291
SB 202190 (p38-inhibitor)	MilliporeSigma	Cat# S7067
Meta-Iodobenzylguanidine (MIBG)	MilliporeSigma	Cat# 19890
Tamoxifen (TAM)	MilliporeSigma	Cat# T5648-5G
TAM diet	Envigo	Cat# TD.130857

REAGENT or RESOURCE	SOURCE	IDENTIFIER
RIPA Protein Lysis Buffer	Thermo Fisher	Cat# 89900
Trizol Reagent	Thermo Fisher	Cat# 15596026
Polybrene	MilliporeSigma	Cat# TR-1003
Puromycin	MilliporeSigma	Cat# P9620
Hygromycin B solution	Millipore Sigma	Cat# H0654
Doxycycline Hyclate	Epic Pharma	Cat# NDC 42806312-05
0.5M EDTA, pH 8.0	Millipore Sigma	Cat# 03690
0.5M EGTA, pH 8.0	Boston Bioproducts	Cat# BM-151
Cardiotoxin (CTX)	Latoxan	Cat# L8102
HEPES	Millipore Sigma	Cat# H3375
NaCl	Millipore Sigma	Cat# 71376
Formaldehyde Solution, 37%	Millipore Sigma	Cat# F8775
Glycine	Millipore Sigma	Cat# 50046
cOmplete, Mini, EDTA-free Protease Inhibitor Cocktail	Millipore Sigma	Cat# 11836170001
Critical commercial assays		
GeneChIP Mouse Gene 1.0 ST Array	Thermo Fisher	Cat# 901168
SMART-Seq v4 Ultra Low Input RNA Kit	Takara (CloneTech)	Cat# 634890
Nextera XT DNA Library Preparation Kit	Illumina	Cat# FC-131-1096
SuperScript VILO cDNA Synthesis Kit	Thermo Fisher	Cat# 1175050
RNeasy Micro Kit	QIAGEN	Cat# 74004
Power SYBR Green PCR Master Mix	Thermo Fisher	Cat# 4367659
FastStart Universal SYBR Green Master Mix (Rox)	Sigma-Aldrich	Cat# 4913850001
Click-it EdU Alexa Fluor 647 Imaging Kit	Thermo Fisher	Cat# C10337
Trans-IT-LT1 Transfection Reagent	Mirus	Cat# Mir2304
Lipofectamine 2000	Thermo Fisher	Cat# 11668030
Lenti-X Virus concentrator Kit	Takara (Clonetechn)	Cat# 631232
Vector M.O.M Immunodetection Kit	Vector Labs	Cat# BMK-2202
Gateway LR Clonase II Enzyme Mix	Thermo Fisher	Cat# 11791100
iDeal ChIP-qPCR Kit x 24	Diagenode	Cat# C01010180
DiaMAG protein A-coated magnetic beads (ChIP-Seq-grade)	Diagenode	Cat# C03010020
Deposited data		
Raw and analyzed RNA-Seq Data	This study	GEO: GSE119895
Raw and analyzed Microarray Data	This study	GEO: GSE119695
Experimental models: organisms/strains		
Mouse: C57BL/6J	Jackson Labs	Cat# 000664
Mouse: C57BL/10ScSn-Dmd ^{mdx} /J	Jackson Labs	Cat# 001801
Mouse: B6.Cg-Tg(Fos/EGFP)1-3Brth/J	Jackson Labs	Cat# 014135
Mouse: B6.Cg-Gt(ROSA) 26Sor ^{flm9(CAG-tdTomato)Hze} /J	Jackson Labs	Cat# 007909

REAGENT or RESOURCE	SOURCE	IDENTIFIER
Mouse: B6.Cg-Pax7 ^{tm1(cre/ERT2)Gaka/J}	Jackson Labs	Cat# 017763
Mouse: Fos ^{fl/fl} (C57BL/6J)	Fleischmann et al., 2003	N/A
Mouse: C57BL/Ka- β -actin-EGFP	Wright et al., 2001	N/A
Oligonucleotides		
Primers for qRT-PCR and cloning, Table S4	This study	N/A
Recombinant DNA		
pMD2.G	N/A	Gift from Didier Trono, Addgene #12259
psPAX2	N/A	Gift from Didier Trono, Addgene #12260
pLKO.1_Art1_shRNA_1	Dharmacon	TRCN0000110341
pLKO.1_Art1_shRNA_2	Dharmacon	TRCN0000110342
pLKO.1_Non-targeting_shRNA	Dharmacon	RHS6848
pEN_TTmcs	Shin et al., 2006	Addgene # 25755
pSLIK_Hygro	Shin et al., 2006	Addgene # 25737
pMDLg/pRRE	Dull et al., 1998	Gift from Didier Trono, Addgene # 12251
pRSV-REV	Dull et al., 1998	Gift from Didier Trono, Addgene # 12253
pCMV-VSV-G	Dull et al., 1998	Gift from Didier Trono, Addgene # 8454
Software and algorithms		
R statistical programming environment	https://www.r-project.org	Version R 3.5.1
RMS (R-package)	N/A	Version 5.1–2
Limma (R-package)	Ritchie et al., 2015	Version 3.36.3
STAR: RNA-Seq aligner	Dobin et al., 2013	Version 2.5.0
HT-Seq	Anders et al., 2015	Version 0.6.1
DeSeq2 (R-package)	Love et al., 2014	Version 1.20.0
DAVID Bioinformatics	https://david.ncifcrf.gov	Version 6.8
Enrichr	Kuleshov et al., 2016	N/A
GeneOverlap (R-package)	https://bioconductor.org/packages/release/bioc/html/GeneOverlap.html	Version 1.16.0
Figi (ImageJ)	https://fiji.sc	N/A
Other		
Raw Microarray Data	Liu et al., 2013	GEO: GSE47177
Raw RNA-Seq Data	Ryall et al., 2015	GEO: GSE64379
Raw RNA-Seq Data	Charville et al., 2015	ENA: PRJEB10091
Processed H3K27ac ChIP-Seq Data	Machado et al., 2017	GEO: GSE103163